Rotation of the Milky Way and the formation of the Magellanic Stream

Adam Růžička[1] and Christian Theis[2]
Institut für Astronomie der Universität Wien, Türkenschanzstrasse 17, A-1180 Wien, Austria
adam.ruzicka@univie.ac.at
and

Jan Palouš
Astronomical Institute of the Academy of Sciences of the Czech Republic, Boční II 1401, 14131 Praha

ABSTRACT

We studied the impact of the revisited values for the LSR circular velocity of the Milky Way (Reid et al. 2004) on the formation of the Magellanic Stream. The LSR circular velocity was varied within its observational uncertainties as a free parameter of the interaction between the Large (LMC) and the Small (SMC) Magellanic Clouds and the Galaxy. We have shown that the large–scale morphology and kinematics of the Magellanic Stream may be reproduced as tidal features, assuming the recent values of the proper motions of the Magellanic Clouds (Kallivayalil et al. 2006). Automated exploration of the entire parameter space for the interaction was performed to identify all parameter combinations that allow for modeling the Magellanic Stream. Satisfactory models exist for the dynamical mass of the Milky Way within a wide range of $0.6 \cdot 10^{12}\,\mathrm{M}_\odot$ to $3.0 \cdot 10^{12}\,\mathrm{M}_\odot$ and over the entire 1–σ errors of the proper motions of the Clouds. However, the successful models share a common interaction scenario. The Magellanic Clouds are satellites of the Milky Way, and in all cases two close LMC–SMC encounters occurred within the last 4 Gyr at $t < -2.5\,\mathrm{Gyr}$ and $t \approx -150\,\mathrm{Myr}$, triggering the formation of the Stream and of the Magellanic Bridge, respectively. The latter encounter is encoded in the observed proper motions and inevitable in any model of the interaction. We conclude that the tidal origin of the Magellanic Stream implies the introduced LMC/SMC orbital history, unless the parameters of the interaction are revised substantially.

Subject headings: galaxies: evolution — galaxies: interactions — galaxies: kinematics and dynamics —Magellanic Clouds — methods: numerical

1. Introduction

Modeling the evolution of the Magellanic Clouds and their interaction with the Milky Way is a challenging task. We have to deal with a unique system of nearby galaxies which have been subject to various detailed observational surveys. The resulting amount of data has established an extended set of constraints for every theoretical study of the formation and evolution of the Magellanic Clouds. On the other hand, namely the information about the kinematics and the morphology of the large–scale structures associated with the Clouds have proved useful to reduce significantly the parameter space of the interaction between the Large Magellanic Cloud (LMC), the Small Magellanic Cloud (SMC) and the Milky

[1]also Astronomical Institute of the Academy of Sciences of the Czech Republic, Boční II 1401, 14131 Praha

[2]present address: Planetarium Mannheim, Wilhelm–Varnholt–Allee 1 (Europaplatz), 68165 Mannheim, Germany

Way.

Undoubtedly, the spatial velocities of the Magellanic Clouds are the most critical input parameters for models of their interaction (Růžička et al. 2009). Regarding the difficulties accompanying the observational measurements of the proper motions of the LMC and the SMC, it is not surprising that the results have always suffered from large uncertainties (see, e.g. Kroupa & Bastian 1997; Pedreros et al. 2002). Thus, the most important parameters were also the most uncertain ones.

A common feature of models of the Magellanic Clouds (see Section 2) are bound orbits around the Galaxy, with several revolutions over the Hubble time. However, recent proper motion measurements by Kallivayalil et al. (2006b,a) have introduced entirely surprising results. Besides a substantial reduction of the errors, they claim significantly increased galactocentric velocities. The subsequent detailed analysis by Besla et al. (2007) has revealed a new value of the LMC galactocentric velocity $v_{\rm LMC} \approx 350\,{\rm km\,s^{-1}}$, which is close to the local escape velocity. Thus, the scenario with several perigalactic approaches has become rather unlikely.

Through a detailed automated exploration of the parameter space, Růžička et al. (2009) have shown that the new data by Kallivayalil et al. (2006b,a) rule out tidal stripping as the process possibly dominating the formation of the Magellanic Stream – a gaseous trailing tail emanating from the Magellanic Clouds, crossing the South Galactic Pole and stretched over $\approx 100^\circ$ of the plane of sky. Mastropietro (2009) later claimed that the efficiency of ram pressure increased due to the higher relative velocity of the Clouds and the hot halo gas. This might compensate for the shorter timescale for the interaction, and allow for the creation of the Magellanic Stream of a spatial extent comparable to the observations.

The analysis of the orbital history of the LMC by Shattow & Loeb (2009) allowing for the modified values of the LSR circular velocity Θ_0 and the LSR angular rotation rate Ω_0 (Reid & Brunthaler 2004) has introduced promising results. The combination of changes to both, the kinematics and dynamics of the interaction, may result in the decrease of the total energy of the LMC–Milky Way pair, and keep the LMC within the tidal radius of the Galaxy for several Gyrs.

Following the findings by Shattow & Loeb (2009), we have investigated the dynamical evolution of the Magellanic Clouds and their interaction with the Galaxy in terms of a fully automated exploration of the parameter space for the interaction. The goal of this study is to show whether the up–to–date observational estimates of the LMC/SMC proper motions together with the revisited values for the solar galactocentric motion and distance allow for the reproduction of the large–scale distribution of neutral hydrogen (H I) in the LMC–SMC–Milky Way system (the Magellanic System) due to the gravitational tidal stripping. The approach applied was introduced by Růžička et al. (2007, 2009), and it is based on the evolutionary optimization (genetic algorithm) of the model input according to its ability to reproduce the H I observations of the Magellanic System (Brüns et al. 2005).

The procedure devised by Růžička et al. (2009) was followed with a couple of modifications. The ranges of the proper motions of the Clouds were redefined in order to accommodate not only the data by Kallivayalil et al. (2006b,a) but also the results by Piatek et al. (2008) who reprocessed independently the original raw proper motion data (Figure 1). The parameter space of the LMC–SMC–Milky Way interaction was also extended by an additional dimension representing the LSR circular velocity. A more detailed description of the studied parameter space will be provided in Section 3.

The reader familiar with the papers by Růžička et al. (2007, 2009) may skip Section 4 which introduces the technical details of our numerical model and the principles of the automated exploration of parameter spaces. In Section 5 the influence of the LSR circular velocity on the interaction between the Magellanic Clouds and the Galaxy is studied. Section 6 offers our results which are later summarized in Section 7, followed by a discussion in Section 8. Finally, the most challenging open questions related to the formation of the large–scale Magellanic structures are mentioned in Section 9.

2. Models of the Magellanic System

It has been a common practice in the theoretical studies of the Magellanic System to adopt sev-

eral reasonable assumptions on the orbital paths of the Clouds to reduce the volume of the current LMC/SMC velocity space. In most cases the Magellanic Stream has been used as a tracer of the past orbits of the Magellanic Clouds (e.g. Fujimoto & Sofue 1976; Gardiner et al. 1994; Connors et al. 2006).

This approach has allowed for remarkably good models of the large–scale distribution of H I in the Magellanic System. Connors et al. (2006) devised a complex tidal model of the interaction between the Clouds and the Milky Way offering an impressive reproduction of the kinematics of H I in the Magellanic Stream. An over–density was present at the tip of the Stream, however, demonstrating the common problem of the tidal stripping.

Alternatively, ansatz explaining the origin of the Stream by the ram pressure stripping of the LMC/SMC neutral hydrogen has been introduced as an explanation. The advanced numerical models by Bekki & Chiba (2005) and Mastropietro et al. (2005) simulated the distribution of H I at the main body of the LMC and the global morphology of the Magellanic Stream. Bekki & Chiba (2005) described the LMC as a system of self–gravitating particles. To account for the dissipative processes in the gaseous medium, the method of sticky particles was employed. The SPH code by Mastropietro et al. (2005) allowed the redistribution of H I in the Clouds to occur at timescales of the order 10^8 yr only.

3. Parameter space of the Magellanic System

Various aspects of modeling observed interacting galaxies were discussed to a great detail in the studies by Theis (1999) or Theis & Kohle (2001). Obviously, even an interaction of two galaxies described in a strongly simplified manner involves well over 10 parameters necessary to describe the structure, the total mass and the mass distribution of both galaxies, and also their initial positions and velocities. In principle, the values of the parameters may be derived from observational data. However, regarding distances of galaxies, acquiring observational data of the resolution and variety sufficient to uniquely determine the parameters of their interactions is very difficult. Unfortunately, this is true even for the satellites of the Milky Way. Thus, modeling interacting galaxies involves inevitably an exploration of the parameter space for the interaction to determine the parameter combinations, i.e. the evolutionary scenarios, compatible with the observed kinematics and morphology of the galactic system.

3.1. Key parameters

The number of parameters required to describe the interaction involving the Milky Way, the LMC and the SMC depends on the physical model adopted. We have employed a restricted N–body numerical code assuming the gravitational interaction only. Even such a simplified view of the interaction involves $\approx$ 25 independent parameters including the initial conditions of the LMC and the SMC motion, their total masses, parameters of mass distributions, particle disk radii, and orientation angles, and also the parameters defining the gravitational potential of the Milky Way, i.e. the flattening parameter of the dark matter (DM) halo, the LSR circular velocity and the LSR angular rotation rate (see Section 5). Some of the parameters were constrained by theoretical studies (including scale radii ϵ of the LMC/SMC halos, the Coulomb logarithm Λ for the dynamical friction in the Milky Way halo, and the halo flattening parameter q for the model of the gravitational potential of the Galaxy). Their mean values and searched errors were discussed in Růžička et al. (2007). This section introduces the observationally estimated parameters of the LMC–SMC–Galaxy interaction (see also Table 1).

It has been shown by Růžička et al. (2009) that the current proper motions of the Magellanic Clouds are the most critical parameters of their interaction with the Milky Way. Figure 1 shows the proper motions of the LMC and the SMC as estimated by the latest analysis by Kallivayalil et al. (2006b,a) and Piatek et al. (2008) based on the measurements by the HST. For convenience, the LMC/SMC proper motion vectors are decomposed into two components related to the local directions of west ($\mu_{\rm W}$) and north ($\mu_{\rm N}$). The reason for involving two results derived from a single data–set is the discrepancy between the studies by Kallivayalil et al. (2006a) and Piatek et al. (2008) regarding the SMC western proper motion $\mu_{\rm W}$. The resulting proper motion space for the Magellanic Clouds explored in this study is a union

of the sets defined by the 1–σ errors of the data by Kallivayalil et al. (2006b,a) and Piatek et al. (2008) for the LMC and the SMC, respectively (Figure 1):

$$\begin{aligned} \mu_{\rm W}^{\rm lmc} &= \langle -2.11, -1.92 \rangle \,{\rm mas\,yr^{-1}} \\ \mu_{\rm N}^{\rm lmc} &= \langle +0.39, +0.49 \rangle \,{\rm mas\,yr^{-1}} \\ \mu_{\rm W}^{\rm smc} &= \langle -1.34, -0.69 \rangle \,{\rm mas\,yr^{-1}} \\ \mu_{\rm N}^{\rm smc} &= \langle -1.35, -0.99 \rangle \,{\rm mas\,yr^{-1}}. \end{aligned} \quad (1)$$

Detailed analysis by Růžička et al. (2009) has quantified the sensitivity of the dynamical evolution of the Magellanic System to the variation in different free parameters. Except the LMC/SMC current spatial velocities and positions, the remaining parameters had a rather weak impact on the interaction. As long as the parameters are independent adding another parameters to the original set does not change the conclusion by Růžička et al. (2009) regarding their importance. However, once parameter independence cannot be guaranteed, it is a good practice to keep the dimensionality of the parameter space as high as possible. Therefore, we will introduce the LSR circular velocity as a new dimension of the Magellanic parameter space established in the way similar to Růžička et al. (2007, 2009).

Unlike the proper motion of the Clouds their LSR radial velocities could be measured with high accuracy. Following van der Marel et al. (2002) we set $v_{\rm rad}^{\rm lmc} = 262.2 \pm 3.4\,{\rm km\,s^{-1}}$. The SMC radial velocity error was estimated by Harris & Zaritsky (2006) as $v_{\rm rad}^{\rm smc} = 146.0 \pm 0.60\,{\rm km\,s^{-1}}$.

The heliocentric position vector of the LMC was adopted from van der Marel et al. (2002), i.e. the equatorial coordinates are $(\alpha_{\rm lmc}, \delta_{\rm lmc}) = (81.90^\circ \pm 0.98^\circ, -69.87^\circ \pm 0.41^\circ)$, its distance modulus is $(m-M)_{\rm lmc} = 18.5 \pm 0.1$. The equatorial coordinates of the SMC were set to the ranges $(\alpha_{\rm smc}, \delta_{\rm smc}) = (13.2^\circ \pm 0.3^\circ, -72.5^\circ \pm 0.3^\circ)$ (see Stanimirović et al. 2004, and references therein). A range of distance determinations for the SMC was provided by van den Bergh (2000) and we used his resulting distance modulus $(m-M)_{\rm smc} = 18.85 \pm 0.10$.

Several observational determinations of the LMC disk plane orientation have been published so far (see, e.g. Lin et al. 1995; van der Marel et al. 2002). In our parameter study the LMC inclination i and position angle p and their errors agree with van der Marel et al. (2002), i.e. $i = 34.7^\circ \pm 6.2^\circ$ and $p = 129.9^\circ \pm 6.0^\circ$. As the SMC misses a well defined disk, the orientation and the position angle usually refer to the SMC "bar" defined by Gardiner & Noguchi (1996). Based on the estimates by van den Bergh (2000) or Stanimirović et al. (2004) we adopted the error ranges $i = 60^\circ \pm 20^\circ$ and $p = 45^\circ \pm 20^\circ$ for the SMC initial disk inclination and position angle, respectively.

Gardiner et al. (1994) analyzed the H I surface contour map of the Clouds to estimate the initial LMC and SMC disk radii $r_{\rm disk}^{\rm lmc}$ and $r_{\rm disk}^{\rm smc}$, respectively. With the use of their work and of the study by Brüns et al. (2005) we varied the LMC/SMC disk radii within the ranges of 10.5 ± 1.5 kpc (LMC) and 6.5 ± 1.5 kpc (see Table 1). Regarding the absence of a clearly defined disk of the SMC and possible significant mass redistribution in the Clouds during their evolution, the results require careful treatment.

Current total masses $m_{\rm lmc}$ and $m_{\rm smc}$ follow the estimates by van den Bergh (2000). The masses of the Clouds are functions of time and evolve due to the LMC–SMC exchange of matter and as a consequence of the interaction between the Clouds and the MW. Our test–particle model does not allow for a reasonable treatment of a time–dependent mass loss. Therefore, the masses of the Clouds are considered constant in time and their initial values at the starting epoch of simulations are approximated by the current LMC and SMC masses.

The gravitational potential of the Milky Way is modeled by the superposition of three static components including the axially symmetric logarithmic potential (Binney & Tremaine 1987) of the DM halo, the Miyamoto–Nagai potential of the Galactic disk, and the Hernquist bulge. Since the logarithmic halo is the dominant component of our model, its flattening parameter was treated as a free parameter. The flattening q was varied within the range of $\langle 0.71, 1.30 \rangle$. The lower limit is based on the condition $q > 1/\sqrt{2}$ required to avoid negative mass densities in the logarithmic halo. The upper limit was set up to introduce a convenient symmetry with respect to the spherical shape ($q = 1$). The scaling velocity factor v_0 of the logarithmic model (more details in Binney & Tremaine 1987) is a function of the LSR circular velocity and the solar galactocentric dis-

tance.

The freedom in the values of the parameters q and v_0 introduced a spread in the total mass of the Galaxy $m_{\rm MW} = \langle 0.59, 5.90\rangle \cdot 10^{12}\,{\rm M}_\odot$ within the radius of 250 kpc. The estimates of the total mass of the Milky Way exceeding $\approx 3 \cdot 10^{12}\,{\rm M}_\odot$ have neither observational not theoretical support (see e.g. Binney & Tremaine 1987; Li & White 2008), but this fact will be taken into account when the results are interpreted.

3.2. Rotation curve of the Milky Way

Unlike the studies by Růžička et al. (2007, 2009) we have treated the LSR circular velocity Θ_0 as a free parameter. This decision was motivated by recent findings by Reid & Brunthaler (2004). Their measurements of the proper motion of Sag A* yielded the estimate for the LSR circular velocity $\Theta_0 = 236 \pm 15\,{\rm km\,s^{-1}}$. At the same time, they give a revisited value of the LSR angular rotation rate Ω_0 of $29.45\,{\rm km\,s^{-1}\,kpc^{-1}}$. These two quantities then define the variations of the solar galactocentric distance, as $R_0 = \Theta_0/\Omega_0$.

Reid & Brunthaler (2004) performed very precise position measurements of the famous radio source Sag A* with respect to two background extragalactic radio sources. The data collected over a period of 8 years yielded values of the apparent motion of Sag A*. This quantity is a composition of the reflected solar galactocentric motion and of the peculiar motion of Sag A* which is quite small. The fraction of the apparent motion corresponding to Solar rotation around the Galactic Center may be treated as a combination of the Local Standard of Rest (LSR) circular velocity Θ_0 and the deviation of the solar motion from the circular orbit (Dehnen & Binney 1998). Finally, Reid & Brunthaler (2004) were able to determine the latter which yielded an estimate for the LSR circular velocity $\Theta_0 = 236 \pm 15\,{\rm km\,s^{-1}}$ assuming the solar distance to the Galactic center (R_0) of 8.0 ± 0.5 kpc. Notably, the uncertainty of Θ_0 originating from the measurement error was only $1\,{\rm km\,s^{-1}}$. The rest appears due to the uncertainty of R_0 (Reid & Brunthaler 2004). Calculating the LSR angular rotation rate $\Omega_0 \equiv \Theta_0/R_0$ yields a value with a very small uncertainty: $\Omega_0 = 29.45 \pm 0.15\,{\rm km\,s^{-1}\,kpc^{-1}}$. The corresponding relative error is only $0.15/29.45 = 5 \cdot 10^{-3}$ which is by one order of magnitude below the relative error of any of the parameters examined in our study. Therefore, the LSR angular rotation rate Ω_0 will be treated as a constant in this paper, i.e. $\Omega_0 = 29.45\,{\rm km\,s^{-1}\,kpc^{-1}}$.

Although we are already familiar with the impact of most of the discussed parameters on the behavior of the restricted N–body model of the LMC–SMC–Milky Way interaction (see Růžička et al. 2009), this does not apply on the LSR circular velocity. Even though it is a natural choice, taking the 1–σ error box of Θ_0 by Reid & Brunthaler (2004) for the range explored by the parameter study is arguably not a good practice. We want to avoid the case of important models being localized at either end of the studied parameter range. Such a coincidence would then require an extension of the studied range of the LSR circular velocity followed by another time–consuming run of the automated parameter search. The described procedure is necessary to uncover and understand the behavior of the interacting system in such a parameter region of apparently special features. Therefore, the range of the new input parameter Θ_0 was obtained by extending the 1–σ uncertainty of the LSR circular velocity as published in Reid & Brunthaler (2004) by $10\,{\rm km\,s^{-1}}$, i.e. $\Theta_0 = \langle 210, 260\rangle\,{\rm km\,s^{-1}}$, corresponding to the range of the Solar galactocentric distance R_0 of $\langle 7.13, 8.83\rangle$ kpc.

4. Method

This paper focuses on the gravitational interaction between the Magellanic Clouds and the Milky Way. Although hardly any doubts exist regarding the presence of the hydrodynamical processes, as the LMC/SMC neutral hydrogen interacts with the ambient hot gas of the Galactic halo, the tidal stripping is intrinsically involved in every model assuming the gravitational interaction.

4.1. Restricted N–body model

The model itself is an advanced version of the scheme by Gardiner et al. (1994): it is a restricted N–body (i.e. test particle) code describing the gravitational interaction between the Galaxy and its dwarf companions. The potential of the Milky Way is dominated by the flattened dark matter halo and dynamical friction is exerted on the Magellanic Clouds as they move through the

halo (Binney 1977). The LMC and the SMC are represented by Plummer spheres, initially surrounded by test–particle disks. For further details see Růžička et al. (2007, 2009).

4.2. Searching the parameter space

The exploration of the parameter space for the interaction involving the Galaxy and the Magellanic Clouds was performed by a genetic algorithm. Genetic algorithms belong to the class of evolutionary optimizers that mimic the selection strategy of natural evolution. Holland (1975) was the first one who proposed the application of genetic algorithms on optimization problems in mathematics. Recently, the performance of genetic algorithms was studied for galaxies in interaction (see, e.g. Theis 1999). Theis & Kohle (2001) analyzed the parameter space of two observed interacting galaxies – NGC 4449 and DDO 125. Genetic algorithms turned out to be very robust tools for such a task if the routine comparing the observational and modeled data is appropriately defined. The approach by Theis & Kohle (2001) was later adopted and improved in order to explore the interaction of the Magellanic Clouds and the Galaxy (Růžička et al. 2007, 2009).

The comparison between the model and observations became more efficient by involving an explicit search for the shapes in the data (Růžička et al. 2009). Also the significant system–specific features (such as a special geometry and kinematics) were taken into account, further improving the performance of the genetic algorithm for exploration of the LMC–SMC–Galaxy interaction. More detailed information is to be found in Section 4.3 of this paper.

4.3. Fitness function

The automated search of the parameter space is driven by a routine comparing the modeled and observed distributions of H I associated with the Magellanic System (Brüns et al. 2005). The match is measured by the *fitness function* (f) which is a function of all input parameters, as every parameter set determines the resulting simulated H I data–cube. Our fitness function returns a floating–point number between 0.0 (complete disagreement) and 1.0 (perfect match) and consists of four different comparisons, including search for structures and analysis of local kinematics. For details on the fitness function used for this study see Appendix A.

The fitness function f is the only part of the genetic algorithm that reflects the nature of the studied problem. Although the automated evolutionary optimization is a robust method applicable on a remarkable variety of systems, its actual performance and efficiency are critically dependent on the proper choice for the fitness function. If the function is defined in a sensible way, the number of parameter combinations examined by the genetic algorithm is minimized. However, the performance of the genetic algorithm also depends on its convergence rate expressed as $d\overline{f}(i)/di$, where $i = 1, 2, ...$ stands for the number of the actual generation and $\overline{f}(i)$ is the mean value of the fitness function in the i–th generation. The convergence rate is generally proportional to the ratio of the generation size $N_{\rm gen}$ and of the dimension n of the studied parameter space over which the fitness function is defined. Unfortunately, the value of $N_{\rm gen}/n$ is very low if genetic algorithm–based optimizer is applied on the parameter spaces of interacting galaxies. The number of parameters involved is always high (see Section 3). On the other hand, the maximum generation size has to be limited in order to keep the total computational time requested by the parameter search reasonable.

In order to overcome such a difficulty we searched the parameter space repeatedly in a fixed number of optimization steps, i.e. generations of models, and localized ≈ 100 high–fidelity models. Such a procedure is not likely to reveal the global maximum of the fitness function, but it results in a map of distribution of good models over the entire parameter space. In principle, every region of the parameter space allowing for the satisfactory reproduction of the large–scale structures associated with the Magellanic Clouds may be identified.

The reader might ask why there is such emphasis placed on the fitness function itself if it, in fact, does not seem to provide any physical information about the interacting system of the Galaxy and the Magellanic Clouds. Indeed, the function f serves primarily as a driver to the genetic algorithm. However, the search for good models of the observed Magellanic System is efficient only if relevant astrophysical data are supplied as the input

to f. As already mentioned, our study deals with detailed morphological and kinematic information from the 21 cm survey by Brüns et al. (2005) and with the corresponding modeled data. The fitness function then makes a link between the observable data and the initial state of the Magellanic System.

5. The role of the Solar galactocentric velocity and distance

The conclusions by Reid & Brunthaler (2004) regarding the LSR angular rotation rate Ω_0 and the LSR circular velocity Θ_0 have a significant impact on both the kinematics and the dynamics of the Magellanic System.

The dynamics of the interaction between the Magellanic Clouds and the Galaxy is influenced by the change of the mass distribution and of the total mass of the Milky Way. The value of Ω_0 by Reid & Brunthaler (2004) implies that the IAU standards for Θ_0^{IAU} and for the Solar galactocentric distance R_0^{IAU} cannot hold at the same time anymore, as

$$\Omega_0^{\mathrm{IAU}} = \frac{\Theta_0^{\mathrm{IAU}}}{R_0^{\mathrm{IAU}}} = \frac{220\,\mathrm{km\,s^{-1}}}{8.5\,\mathrm{kpc}} = 25.88\,\mathrm{km\,s^{-1}\,kpc^{-1}},$$

while Reid & Brunthaler (2004) expect that $\Omega_0 = 29.45\,\mathrm{km\,s^{-1}\,kpc^{-1}}$. Therefore, a rescaling of the rotation curve of the Galaxy occurs if the results by Reid & Brunthaler (2004) are taken into account, which necessarily means a rescaling of the mass distribution in the Galaxy.

The current positions of the Magellanic Clouds in the phase space have been measured with respect to the phase space position of the Sun. In order to solve the equations of motion for the interaction between the Clouds and the Milky Way, the galactocentric positions and velocities of the LMC and the SMC are needed, i.e. the knowledge in the LSR circular velocity Θ_0 and the LSR galactocentric distance R_0 is necessary (see Figure 2). Thus, it is obvious that the results by Reid & Brunthaler (2004) may influence the kinematics of the Magellanic Clouds.

5.1. Model of the Milky Way

The rotation curve of a galaxy

$$v^2(R) = R \left| \frac{\partial \Phi_{\mathrm{tot}}(R,z)}{\partial R} \right|_{z=0} \qquad (2)$$

introduces a fundamental constraint on the models of its overall potential $\Phi_{\mathrm{tot}}(R,z)$. In our study, the following three component model of the potential of the Milky Way has been used:

$$\Phi_{\mathrm{tot}}(R,z) = \Phi_{\mathrm{L}}(R,z) + \Phi_{\mathrm{MN}}(R,z) + \Phi_{\mathrm{B}}(r), \quad (3)$$

where

$$\Phi_{\mathrm{L}}(R,z) = \frac{1}{2} v_0^2 \ln\left(R_{\mathrm{c}}^2 + R^2 + \frac{z^2}{q^2}\right) \qquad (4)$$

is the logarithmic model of the Galactic DM halo,

$$\Phi_{\mathrm{MN}}(R,z) = -\frac{GM_{\mathrm{d}}}{\sqrt{R^2 + \left(b + \sqrt{z^2 + c^2}\right)^2}} \qquad (5)$$

is the Miyamoto–Nagai potential of the Galactic disk with the total mass M_{d}, and

$$\Phi_{\mathrm{B}}(r) = -G\frac{M_{\mathrm{b}}}{r + a} \qquad (6)$$

is the Hernquist formula for the spherically symmetric potential of the Milky Way bulge with the mass M_{b}.

At the galactocentric distance where the Magellanic Clouds have resided, i.e. $D \gtrapprox 50\,\mathrm{kpc}$, the gravitational field of the Galaxy is dominated by its DM halo component. The role of the DM halo becomes more prominent with the increasing distance to the galactic center, because $\nabla\Phi_{\mathrm{L}} \sim 1/r$ while $\nabla\Phi_{\mathrm{MN}} \sim 1/r^2$ and also $\nabla\Phi_{\mathrm{B}} \sim 1/r^2$. The necessary adjustment of the Milky Way potential Φ_{tot} required by the Equation (2), if the LSR circular velocity Θ_0 is changed, was achieved by varying the velocity constant v_0 in Equation (4).

The choice for the remaining parameters in the Equations (4), (5), and (6) follows Fellhauer et al. (2006) and Růžička et al. (2007, 2009) and so we have set $a = 0.7\,\mathrm{kpc}$, $b = 6.5\,\mathrm{kpc}$, $c = 0.26\,\mathrm{kpc}$, $M_{\mathrm{b}} = 3.4\,10^{10}\,\mathrm{M_\odot}$, $M_{\mathrm{d}} = 10^{11}\,\mathrm{M_\odot}$, and $R_{\mathrm{c}} = 12.0\,\mathrm{kpc}$.

The value of the characteristic radius R_{c} determining the concentration of the Galactic halo is five times smaller than the present galactocentric distances of the Magellanic Clouds, and by the order of 10 smaller compared to the typical LMC/SMC galactocentric distances over the last several Gyr. Hence, its impact on the density profile of the region of the DM halo of the Milky Way, where the Clouds have resided, is weak. Regarding the total mass of the Galaxy enclosed within

a given radius, it is determined by the velocity parameter v_0, as

$$m_{\rm MW} = \int_{\rm halo} \rho_{\rm L}(R,z,q) d^3\mathbf{r} + M_{\rm b} + M_{\rm d}, \quad (7)$$

where the density of the logarithmic halo of the Galaxy $\rho_{\rm L}(R,z) \sim v_0^2$, while $\rho_{\rm L}(R,z) \sim 1/R_{\rm c}^2$. We did not consider the scale radius $R_{\rm c}$ as a free parameter because its influence on the mass distribution and the total mass of the DM halo of the Milky Way is significantly lower compared to the velocity parameter v_0.

The flattening q of the DM halo potential entered our simulations of the Magellanic System as a free parameter (see Sec. 3). The velocity parameter v_0 of the logarithmic halo was considered a function of the LSR circular velocity Θ_0. The corresponding formula comes out of the Equations (2) and (3) after substituting for $\Phi_{\rm L}$, $\Phi_{\rm MN}$, and $\Phi_{\rm B}$:

$$\begin{aligned} v_0^2 &= \Theta_0^2 \left(1 + \frac{R_{\rm c}^2}{R_0^2}\right) - G\left(R_{\rm c}^2 + R_0^2\right) \\ &\cdot \left[\frac{M_{\rm d}}{\left(R_0^2 + (b+c)^2\right)^{1.5}} + \frac{M_{\rm b}}{R_0 (R_0 + a)^2}\right] \end{aligned} \quad (8)$$

where $R_0 = \Theta_0/\Omega_0$.

The analysis of the Equation (8) shows that if

$$a < \Theta_0/\Omega_0 \quad (9)$$

and

$$(b+c-\sqrt{1.5}R_{\rm c})(b+c+\sqrt{1.5}R_{\rm c}) < 0.5\Theta_0^2/\Omega_0^2 \quad (10)$$

then

$$\frac{\partial v_0^2}{\partial \Theta_0} > 0.$$

It can be easily seen that the conditions (9) and (10) are always satisfied for the values of the parameters a, b, c, and $R_{\rm c}$ assumed in our study. As we have Equation (7) for the logarithmic halo (Binney & Tremaine 1987), the total mass of the Milky Way enclosed within an arbitrary radius r must grow if the LSR circular velocity Θ_0 is increased.

5.2. Galactocentric positions and velocities of the Magellanic Clouds

A convenient transformation of the position and velocity vectors of the Magellanic Clouds from the heliocentric spherical coordinates to the galactocentric Cartesian frame (Figure 2) was derived by van der Marel et al. (2002). Let (l, b) and (α, δ) be the corresponding pair of the galactic and equatorial coordinates of the center of mass of either of the Magellanic Clouds, respectively. If the Cloud's present heliocentric distance is D, its galactocentric Cartesian coordinates are

$$r^i = R_\odot^i + D u_0^i, \quad i = 0, 1, 2, \quad (11)$$

where $\mathbf{R}_\odot$ is the Solar galactocentric position vector and $\mathbf{u_0}$ is the heliocentric unit position vector of the Cloud.

The heliocentric spatial velocity of an object in space is usually expressed in terms of its proper motion and the line–of–sight systemic velocity $v_{\rm sys}$. The proper motions in the directions of west and north are defined as (van der Marel et al. 2002)

$$\mu_{\rm W} = -\cos\delta \frac{d\alpha}{dt}, \quad \mu_{\rm N} = \frac{d\delta}{dt}. \quad (12)$$

The transformation from the heliocentric velocity coordinates $\mu_{\rm W}$, $\mu_{\rm N}$, and $v_{\rm sys}$ to the galactocentric velocity components may be then expressed as

$$v^i = v_\odot^i + v_{\rm sys} u_0^i + D\mu_{\rm W} u_1^i + D\mu_{\rm N} u_2^i, \quad (13)$$

where

$$\begin{aligned} \mathbf{u_0} &= (\cos l \cos b, \sin l \cos b, \sin b) \\ \mathbf{u_1} &= -\frac{1}{\cos\delta}\frac{\partial \mathbf{u_0}}{\partial \alpha} \\ \mathbf{u_2} &= \frac{\partial \mathbf{u_0}}{\partial \delta}, \end{aligned} \quad (14)$$

and $\boldsymbol{v}_\odot$ is the Solar galactocentric velocity vector.

Taking Equations (11) and (13) into account together with the fact that $\mathbf{R}_\odot = (-\Theta_0/\Omega_0, 0, 0)$ and $\boldsymbol{v}_\odot = (0, \Theta_0, 0)$ (see Figure 2), it is obvious that the current galactocentric positions and velocities of the Magellanic Clouds depend on the values of the LSR circular velocity Θ_0 and of the LSR angular rotation rate Ω_0. If either of these two parameters is varied, a change to the galactocentric position vectors of the Clouds occurs due to the change of their x–components:

$$r^0 = -\Theta_0/\Omega_0 + D u_0^0. \quad (15)$$

Similarly, the galactocentric spatial velocities of the LMC and the SMC would be influenced, be-

cause their y–components involve the explicit dependence on Θ_0:

$$v^1 = \Theta_0 + v_{\rm sys} u_0^1 + D\mu_{\rm W} u_1^1 + D\mu_{\rm N} u_2^1. \quad (16)$$

Note that the phase space configuration of the system involving the Sun, the Magellanic Clouds and the Galactic Center is such that $v^1 \sim \Theta_0$, while $|v^1| \sim -\Theta_0$. As a consequence, the magnitude of the galactocentric velocity

$$|\boldsymbol{v}|^2 \sim (\Theta_0 + v_{\rm sys} u_0^1 + D\mu_{\rm W} u_1^1 + D\mu_{\rm N} u_2^1)^2 \quad (17)$$

of the LMC decreases if the LSR circular velocity is increased. Figure 3 reveals clearly that the same conclusion holds for the SMC.

Variation of the LSR circular velocity Θ_0 and of the LSR angular rotation rate Ω_0 modifies both the magnitudes and the directions of the position and velocity vectors of the Clouds. Specifically, increase in the LSR circular velocity causes the reduction of the magnitude of the LMC/SMC galactocentric velocities.

6. Results

The complex nature of the interaction involving the Magellanic Clouds and the Milky Way results in a high–dimensional parameter space. We have studied the parameter space by employing genetic algorithms as robust optimization tools characterized by reliability and low sensitivity to local extremes (Theis & Kohle 2001). This method was adopted to analyze the performance of pure tidal models for the Magellanic System.

Regarding the insufficient convergence rate of our genetic algorithm (see Section 4.3), the automated exploration of the parameter space was performed repeatedly and the properties of the resulting high–fidelity models were analyzed statistically. We have identified the regions of the parameter space where promising models of the LMC–SMC–Milky Way interaction exist.

This paper focuses on the influence of the LSR circular velocity Θ_0 on the formation of the Magellanic Stream provided the current spatial velocities of the Magellanic Clouds respect the recent proper motion data by Kallivayalil et al. (2006b,a) and by Piatek et al. (2008). In particular, we want to address the question of how to choose this parameter in a way that agrees with the recent measurements by Reid & Brunthaler (2004) and allows for the reproduction of the observed kinematics and spatial extent of H I in the Magellanic Stream.

6.1. Exploration of the parameter space

With the use of the genetic algorithm, $\sim 10^6$ parameter combinations, i.e. individual restricted N–body simulations, were examined in total, and ~ 100 sets providing the highest fitness models were collected. In this section the features of these models will be discussed with respect to the parameters influencing the motion of the Magellanic Clouds.

We have treated the LSR circular velocity as a free parameter in order to analyze its impact on the tidal interaction in the Magellanic System. The automated exploration of the modified parameter space revealed a significant qualitative change regarding the preferred proper motions of the Clouds, compared to the work by Růžička et al. (2009).

They have done a detailed analysis of how the models of the LMC–SMC–Galaxy interaction depend on different parameters. It was clearly shown that the interacting system is very sensitive to the parameters defining the past positions of the Clouds' orbits in phase space. In the work by Růžička et al. (2009) the set of the critical parameters involved the current heliocentric positions and velocities of the Magellanic Clouds and, to some extent, the flattening parameter of the Milky Way halo. However, introducing the new value of the LSR angular rotation rate by Reid & Brunthaler (2004) and treating the LSR circular velocity as a free parameter has changed the old picture.

Figure 4 shows the distribution of the local peaks of the fitness function f (i.e. the fitness of every model identified by the genetic algorithm) over the studied ranges of the western and northern components of the proper motions for both Magellanic Clouds. In contrast to Růžička et al. (2009), there is no apparent preference for specific values of the proper motions for either of the Clouds. Models of a very similar quality have been located over the entire studied proper motion ranges of the LMC and the SMC. Notably, the high–fitness models fall into either of two groups

clearly separated by the fitness values of their members. The majority of the models has the fitness exceeding the value of 0.55 while most of the rest are described by the relation $f < 0.50$. Only $\sim 5\%$ of all the models are located within the fitness range of $0.50 < f < 0.55$. Later in Section 6.7 the lower limit for the fitness of the satisfactory models will be precisely established and discussed. For the moment we will just mention that the almost empty belt between the fitness values of 0.50 and 0.55 separates the acceptable models of the Magellanic System from those reproducing the H I observational data by Brüns et al. (2005) insufficiently.

6.2. LSR circular velocity and the halo flattening as parameters

It can be easily seen from Equations (4) and (8) that the LSR circular velocity Θ_0 and the flattening q of the Galactic DM halo determine the total mass of the Milky Way. We have focused on the distribution of all the high–fidelity models of the LMC–SMC–Galaxy interaction over the $q-\Theta_0$ plane of the studied parameter space. Figure 5 visualizes the result. The actual value of the total enclosed mass of the Milky Way does not introduce any limitation regarding the ability of our tidal model to reproduce the observed H I large–scale Magellanic structures. Such behavior exists due to the fact that local peaks of the fitness function (i.e. good models) of a similar quality have been localized over the entire range of the LSR circular velocity.

The distribution of the genetic algorithm fits with respect to the flattening parameter q is quite different. A strong preference for oblate ($q < 1$) configurations of the gravitational potential of the Milky Way halo exists. Such a result agrees with the conclusions by Růžička et al. (2007). In the next paragraphs the role of the LSR circular velocity and the flattening of the Galactic halo will be addressed regarding the impact of these parameters on the orbital history of the Magellanic Clouds.

6.3. Galactocentric velocity of the LMC and the mass of the Milky Way

We have revealed an interesting anti–correlation in the output of the automated parameter search by the genetic algorithm. Figure 6 depicts the relation between the magnitude of the current galactocentric velocity of the LMC and the total mass of the Milky Way for all the high–fitness models. The general trend of the dependence, i.e. the galactocentric velocity of the LMC decreasing as the Galactic mass increases, is driven by the LSR circular velocity Θ_0 due to the way it links the Equations (7), (8) and (17), and together with the fact that the mass of the Milky Way is dominated by the DM halo.

Equation (7) may be expressed as

$$m_{\mathrm{MW}} = \upsilon_0^2(\Theta_0)g(q) + M_{\mathrm{b}} + M_{\mathrm{d}}, \qquad (18)$$

and for the galactocentric velocity we get

$$|\boldsymbol{\upsilon}_{\mathrm{i}}| = h(\Theta_0, \alpha_{\mathrm{i}}, \delta_{\mathrm{i}}, (m-M)_{\mathrm{i}}, \mu^{\mathrm{i}}_{\mathrm{W}}, \mu^{\mathrm{i}}_{\mathrm{N}}, \upsilon^{\mathrm{i}}_{\mathrm{rad}}), \quad (19)$$

where i = lmc. Equations (18) and (19) define the parametric representation of a curve in the $m_{\mathrm{MW}} - |\boldsymbol{\upsilon}_{\mathrm{lmc}}|$ plane. If all parameters except the LSR circular velocity Θ_0 are assumed constant and Θ_0 is varied within the range of $\langle 210, 260\rangle\,\mathrm{km\,s^{-1}}$, the parametric equations yield the curves depicted in Figure 6. The curves are associated with randomly selected high–fitness models by taking their parameter values for the input to Equations (18) and (19). Apparently, the curves are close to linear. Their slope is controlled by the LSR circular velocity and they are well aligned with the distribution of models in the $m_{\mathrm{MW}} - |\boldsymbol{\upsilon}_{\mathrm{lmc}}|$ plane which provides the key to the Figure 6. The distribution of models in the plot is primarily controlled by the LSR circular velocity which sets the linearly decreasing trend of the velocity–mass dependence. The vertical (velocity) and horizontal (mass) placement of the curves depends on the heliocentric positions and velocities of the LMC and on the flattening of the DM halo of the Milky Way respectively.

6.4. Orbits of the Magellanic Clouds

Figure 7 will help us to understand how the variations of the flattening parameter q and of the LSR circular velocity are reflected in the past orbits of the Clouds. One of the parameters was varied within its entire range considered in this study, while the second one was fixed to the value corresponding to a high–fitness model of the interaction.

Figure 7 reveals a qualitative difference in the way the specified parameters affect the motion of the Magellanic Clouds. The influence of the LSR circular velocity is significantly stronger than the role of the flattening of the Galactic potential. This is not surprising. While the flattening parameter only has an impact on the distribution of mass of the Galaxy, variations in the LSR circular velocity also lead to changes of the LMC/SMC galactocentric velocities. Moreover, these effects amplify each other regarding their impact on the orbits of the Clouds (see Section 5). If Θ_0 is increased, the total mass of the Milky Way increases implying a higher gravitational potential energy of the Clouds with respect to the Galaxy. Regarding Equation (17) and the related discussion, the increasing LSR circular velocity reduces the galactocentric velocities of the Clouds, i.e. their kinetic energy. Thus, the total energy of the LMC–Galaxy and the SMC–Galaxy pairs changes with Θ_0 rapidly.

The lower row of Figure 7 shows that the orbits of the Magellanic Clouds projected to the plane of sky are always offset from the position of the Magellanic Stream, regardless of the choice for the $[q, \Theta_0]$ pair. Closer look at Figure 15 reveals that such a deviation is controlled by the northern component $\mu_{\rm N}^{\rm lmc}$ of the LMC proper motion and cannot be removed unless the results by Kallivayalil et al. (2006b,a) and Piatek et al. (2008) are revisited. The particles forming the leading and trailing streams in our restricted N–body model (and generally in every tidal model) essentially follow the orbits of their progenitors. This purely tidal approach is thus limited. As long as the LMC/SMC projected orbits are offset from the observed Magellanic Stream, it is difficult to model the full extent of the large–scale structure of the Stream in the position–position–LSR radial velocity space (see Section 6.8).

Choi et al. (2007) have demonstrated that tidal tails originating in massive satellite galaxies become offset from their progenitors' orbits to some level. However, unless additional physical processes introduce the dissipation of energy and angular momentum of the particles in the tidal tails, such a phase–space deviation between the stream and the orbit of its progenitor is limited. Figure 8 shows how this is reflected by the kinematics of the Magellanic Clouds and the Stream. The high–fitness models are split into the groups of $f > 0.60$ and $f < 0.50$, respectively. It is a common feature of the best models ($f > 0.60$) that the LSR radial velocity along the LMC orbital track agrees well with the famous linear velocity profile of the Magellanic Stream (Brüns et al. 2005).

Despite the previously discussed behavior of tidal models, the apparent offset of the recent ($-300\,{\rm Myr} \lesssim t \leq 0$) LMC/SMC orbits from the Magellanic Stream was reproduced partially by our simulations. It did not occur due to a large deviation between the tidal particle tail and the orbits of the Clouds. The modeled projection of the Magellanic Stream to the plane of sky is still well aligned with the previous revolutions of the LMC/SMC orbits (see Figure 15), but the preceding orbital cycles are projected to different positions in the plane of sky reflecting the geometry and physical properties of the LMC–SMC–Milky Way system.

The subsequent revolutions of the orbits of the Magellanic Clouds are shifted with respect to each other in our good models of the interaction with the Milky Way. This is to be attributed to the projection effect of the configuration of the system involving the observer (Sun), the Galactic Center and the Magellanic Clouds (Figure 2). The flattening of the Galactic potential must be taken into account, as it prevents the LMC from having an orbit confined within a 2 D plane. Figure 9 shows the intensity of the radial and the axial components of the gravitational field of the logarithmic halo. The ratio of the components depends strongly on the position $[R, z]$ with respect to the Galactic Center. That leads to the formation of a 3D orbit of the LMC. We did not mention the SMC, because its low mass makes it dependent not only on the gravitational field of the Galaxy, but also on the attraction by the LMC.

The previous studies of the dynamical evolution of the Magellanic Clouds assumed a good alignment of the LCM/SMC orbits with the Magellanic Stream in the position–position–LSR radial velocity space (see, e.g. Gardiner & Noguchi 1996; Mastropietro et al. 2005; Connors et al. 2006). However, such an assumption is at odds with the HST proper motion measurements for the Clouds (Besla et al. 2007). We have seen that nothing changes even for the revisited values of Θ_0 and Ω_0 by Reid & Brunthaler (2004). What

it represents to modeling the large–scale features of the Magellanic Clouds was briefly discussed in this section and it will be further addressed later in Sections 6.8 and 6.9.

6.5. LMC–SMC encounters

The Magellanic Clouds share a common low–density gaseous envelope (see Brüns et al. 2005) which is usually considered one of the signs indicating that the Clouds have formed a gravitationally bound couple even for several Gyr. Gravitational binding of the Clouds lasting several Gyr turned out to be extremely rare in our simulations. However, the proper motion data by Kallivayalil et al. (2006b,a) and by Piatek et al. (2008) imply that the distance between the LMC and the SMC is very likely to have been shorter than today for several hundred Myr. This may be sufficient to explain the presence of the H I envelope, as our simulations have shown that an envelope surrounding the Magellanic Clouds may be formed rather quickly on the specified time–scale.

The information about the LMC–SMC distance in the recent past comes directly from the combination of Figures 10 and 11. We have calculated the scalar product of the present galactocentric velocity vectors of the Magellanic Clouds for all the high–fitness models. Figure 10 shows the fitness of these models as a function of the actual value of the scalar product. The current LMC and SMC galactocentric velocity vectors are nearly parallel to each other in all cases and their angular deviation does not exceed 20° with the mean value of only $\approx 10°$. It is natural to ask whether the spatial separation of the Clouds is increasing or decreasing at present. Figure 11 offers the answer. If the time dependence of the distance between the Clouds is plotted over the last 700 Myr for the models of $f > 0.55$, one may clearly see that the LMC and the SMC have been receding from one another for ≈ 100 Myr.

To quantify the rate at which the LMC–SMC separation $D_{\mathrm{l-s}}$ changes we have calculated the function $dD_{\mathrm{l-s}}/dt$ at the present time $t = t_0 = 0$ Gyr. If the function $dD_{\mathrm{l-s}}/dt$ is evaluated for the models plotted in Figure 11, it returns the values between 50 kpc Gyr^{-1} and 120 kpc Gyr^{-1}.

The preceding paragraphs lead to the conclusion that the orbital history of the Magellanic Clouds in the high–fitness models always involves a close encounter between the LMC and the SMC at the time of $-250\,\mathrm{Myr} \lesssim t \lesssim -80\,\mathrm{Myr}$. It is quite interesting to see whether such behavior is outstanding or typical within the LMC/SMC proper motion ranges established by the recent HST measurements.

Figure 12 illustrates how the rate at which the current spatial separation of the Magellanic Clouds changes depends on the proper motion of the SMC. We have examined two cases. In one case, the proper motion components of the LMC were fixed to the values of a selected very good model ($f > 0.60$). The model was chosen in such a way that its LMC proper motion components are close to the midpoint values of the intervals established by Equations (1). The SMC proper motion was varied within the entire ranges for $\mu_{\mathrm{W}}^{\mathrm{smc}}$ and $\mu_{\mathrm{N}}^{\mathrm{smc}}$ involved in our study. In all cases, the Magellanic Clouds were found to be receding from one another (Figure 12, left plot), i.e.

$$\frac{dD_{\mathrm{l-s}}}{dt}(\mu_{\mathrm{W}}^{\mathrm{smc}}, \mu_{\mathrm{N}}^{\mathrm{smc}}) > 0. \qquad (20)$$

In the other case, we have kept the values of all the parameters equal to those ones of the mentioned high–fitness model, but the LMC proper motion was modified to reach the minimum galactocentric velocity. Calculating the rate $dD_{\mathrm{l-s}}/dt$ then yielded the result depicted in the right hand plot of Figure 12. Obviously, no change occurred and Equation (20) still holds.

Thus, we have seen that strong support exists for a remarkable feature of the kinematics of the Magellanic Clouds. The recent estimates of the LMC/SMC proper motions by Kallivayalil et al. (2006b,a) and by Piatek et al. (2008) are very likely to introduce a close ($D_{\mathrm{l-s}} \approx 10\,\mathrm{kpc}$) past encounter between the Magellanic Clouds at the time of $\approx -100\,\mathrm{Myr}$ for an arbitrary choice for the LMC/SMC proper motions.

It is reasonable to expect a long–term gravitational binding between the Clouds of the order of 10^9 yr to be a natural condition for repeated encounters in the LMC–SMC system. The corresponding alignment of the past orbital tracks of the Clouds in the phase space requires a very special setup of the parameters for the model of the interacting system, making such a case very un-

likely. However, Figure 13 reveals a surprising picture of the LMC/SMC orbital motion in the deep past. If the separation between the Clouds for the best models ($f > 0.60$) is plotted as a function of time, similar behavior is found in all cases. After the previously discussed close approach a couple of Myr ago, the mutual distance of the Magellanic Clouds reaches 150 kpc, exceeding the value of 200 kpc for some configurations. The Clouds become unbound shortly after their most recent encounter. Nevertheless, every model contains a second close approach at the time $t < -2.5$ Gyr with the separation of the Magellanic Clouds dropping below ≈ 15 kpc. As we will show later, this encounter is the event triggering the formation of an extended trailing tidal tail (the Magellanic Stream) and of its leading counterpart (the Leading Arm).

6.6. Redistribution of mass in the Magellanic System

We have stated in Section 6.1 that only a subset of the models identified by the genetic algorithm in the parameter space may be considered satisfactory reproductions of the observational data (Brüns et al. 2005). In general, an acceptable model of the interaction between the Magellanic Clouds and the Milky Way is supposed to reproduce the extent of the observed Magellanic Stream in the 3 D space composed of the LSR radial velocity and of the position in the plane of sky. The second large–scale H I structure associated with the Clouds – the Leading Arm – is not used to separate good models from the unsuccessful ones.

The Leading Arm appears in tidal models of the LMC–SMC–Galaxy interaction as a natural counterpart of the Magellanic Stream (see Gardiner & Noguchi 1996; Connors et al. 2006), but its acceptable reproduction by the means of numerical simulations remains a challenge. Our parameter study has not changed that picture – the modeled distribution and kinematics of H I in the Leading Arm region and around the main LMC and SMC bodies remains similarly unsatisfactory over the parameter space, especially failing to reproduce the observed morphology of the Leading Arm. In terms of the fitness function, the value of f never exceeds ≈ 0.35 if calculated only for the Leading Arm.

Reliable modeling of the evolution of the central regions of the Magellanic Clouds currently eludes the level of sophistication of our numerical code. The inner parts of the Clouds contain high–density baryonic mass and in order to study their evolution a detailed model involving self–gravity and hydrodynamical processes which account for the mass exchange cycle between stars and gas, is required. Our restricted N–body code overestimates the amount of gas tidally stripped from the LMC/SMC central regions because the tides are not balanced by self–gravity and the dissipative behavior of gas. As a consequence, the modeled column density is lower than observed values in the inner 5 kpc of the Clouds. This effect is stronger in the case of the SMC as it is the dominant source of matter for the Magellanic Stream and the Leading Arm (see Figures 14 or 16). The particle distribution in the LMC is affected by tidal heating by the Milky Way and the original particle disk is turned into a 3 D spherical structure.

6.7. Definition of a good model

The Magellanic Stream turned out to be the appropriate indicator of the quality of our models. Its formation is very sensitive to the choice of the model parameters and critically influences the resulting fitness. Figure 14 illustrates these facts. While the model of $f = 0.61$ is able to fit the basic features of the Magellanic Stream both in the projected H I distribution and the LSR radial velocity profile, a typical simulation representing the model group of $f < 0.50$ places the Magellanic Stream to the position–position–LSR radial velocity space incorrectly. The Stream is extended insufficiently both in position and the LSR radial velocity (upper row of Figure 14), and slope of the simulated profile of the LSR radial velocity along the Stream exceeds the observed one already at the Magellanic longitude of $\approx -30°$ (lower right plot of Figure 14). Generally speaking, the described behavior of the modeled trailing stream is responsible for the resulting fitness of a given model, and was used to define the desired threshold level of the fitness value.

The obvious lack of models within the fitness range of $(0.50, 0.55)$, clearly visible in Figures 4 and 10, was combined with the specified features of the high–fitness models. This yielded the desired threshold level of the fitness function quite

naturally. Figure 4 shows that the fitness of the model establishing the upper limit to the mentioned gap in the distribution of the fitness values lies slightly below 0.55 (it is 0.546 actually). However, the transition between the good and unsatisfactory models is always gradual, as we have seen, and thus the value $f = 0.55$ can be taken for the threshold value of the fitness function with no loss of generality.

6.8. Morphology and kinematics of the Magellanic Stream

In order to discuss our results regarding the reproduction of the large–scale distribution of H I associated with the Magellanic Clouds, we compared a selected high–fidelity model with the low–resolution data–cube of the H I observations by Brüns et al. (2005). The simulated 3 D data–cube depicted in Figure 15 (already shown in Figure 14) was produced by a model with the following values of the LSR circular velocity and the flattening of the Galactic halo: $\Theta = 232\,\mathrm{km\,s^{-1}}$, $q = 0.81$. These values yield the total enclosed mass of the Milky Way within the radius of 250 kpc of $2.20 \cdot 10^{12}\,\mathrm{M}_\odot$.

Assuming the recent measurements of the LMC and the SMC proper motions, our tidal model was able to produce a trailing tail similar to the observed Magellanic Stream regarding both the LSR radial velocity profile and the extent in the projected position. While the LSR radial velocities measured along the Magellanic Stream are reproduced very well, the far tip of the simulated stream at the position of $b \gtrsim -60°$ and $l \approx 70°$ is displaced compared to the observations (Figure 15). Such a displacement appears in every high–fitness model identified by the genetic algorithm in the studied parameter space.

The column density of H I in the Magellanic Stream decreases rather smoothly towards its far tip. This feature exists also in our high–fidelity simulations of the tidally induced formation of the large–scale Magellanic structures. The middle row of Figure 15 shows how the mean H I column density on the line perpendicular to the great circle of the Magellanic longitude (defined in Wannier & Wrixon 1972) changes with the longitude. The simulated profile of the column density (right hand plot) has a steeper slope than the observed Stream and its gradual decrease ends at the Magellanic longitude of $\approx -70°$ compared to $\approx -90°$ for the observations.

The plots in the lower row of Figure 15 also offer the view of the area in the plane of sky where the H I structure called the Leading Arm is located. Brüns et al. (2005) introduced the division of the structure into three systems of gaseous clumps named LA I, LA II and LA III. Their approximate positions in the Galactic coordinates $[b, l]$ are $[-15°, 300°]$ (LA I), $[15°, 290°]$ (LA II), and $[15°, 270°]$ (LA III). The simulation shown in Figure 15 was able to reproduce the part LA III and a fraction of the clump LA II. Some of our high–fitness models offer quite a good match of the overall kinematics and spatial extent for both observed structures LA II and LA III. Nevertheless, no model reproducing both the system LA I and the Magellanic Stream at the same time was found.

6.9. Formation of the Magellanic Stream

It is interesting to take a look at the composition of the simulated Magellanic Stream, and at the process of its build–up over the course of time. The lower left plot of Figure 14 reveals that most of the particles forming the Magellanic Stream in the selected high–fitness model are of the SMC origin. A number of the LMC particles are spread over the full extent of the Stream as well. This is a typical result and it is based on the fact that the LMC particles are more tightly bound due to the significantly higher mass of the LMC compared to the SMC – the LMC:SMC mass ratio is 10:1 in our simulations.

It has already been discussed by Connors et al. (2006) that the Magellanic Stream might consist of several filaments projected to the same region in the plane of sky. Such filaments would be the tidal debris spread along the past orbits of the Clouds. Our study has confirmed such a scenario. Figure 15 shows the projected orbits of the Magellanic Clouds from $t = -3\,\mathrm{Gyr}$ to the present, plotted over the contours of the integrated column density of H I (lower right plot). The SMC has crossed the area currently occupied by the Magellanic Stream three times, while two passages have occurred in case of the LMC. If we disentangle the projected orbital paths, we will find out that the previous orbital revolutions appear more diagonal in our plot. They are placed to lower Galactic lon-

gitudes. The resulting trailing tail is thus a mixture of particles released from the LMC/SMC due to the tidal stripping during several epochs covering the time range from present to $\approx -3.3\,\mathrm{Gyr}$ when the redistribution matter was triggered by a close LMC–SMC encounter.

The complex structure of the modeled Stream can be seen in the lower plot of Figure 16. The LMC/SMC particles are color coded according to the epoch when they were stripped from the Clouds. The Stream and the Magellanic Bridge are dominated by the SMC particles, while most of the LMC particles remain in the vicinity of the main LMC body and have been gradually tidally heated due to the gravitational field of the Milky Way.

The past orbital history of the Magellanic Clouds for the discussed high–fitness model can be seen in the lower plot of Figure 16. For the last 4 Gyr the Clouds have moved within the Galactocentric radius of 200 kpc, undergoing two close ($D_{\mathrm{l-s}} \approx 10\,\mathrm{kpc}$) encounters at the times of $-3.3\,\mathrm{Gyr}$ and $-0.15\,\mathrm{Gyr}$, respectively. The impact of the encounters on the distribution of the LMC/SMC particles was different.

To quantify the influence of the encounters in the LMC–SMC–Galaxy system, we have counted the number of particles shifted from the original orbits of the radius r_i to the distance of $2r_i$ from the center of their progenitor. If this function is evaluated for the time bins of 500 Myr from $t = -4\,\mathrm{Gyr}$, we obtain the upper plot of Figure 16. Apparently, the number of the disturbed particles was increased already in the time bin of $\langle -3.5, -3.0\rangle\,\mathrm{Gyr}$ as a consequence of the first LMC–SMC close approach. This level was later only mildly decreasing, as more of the disturbed particles were stretched in the tidal field of the Milky Way, satisfying the above stated definition of strongly affected particles.

The second close LMC–SMC encounter was significantly more dramatic, disturbing more than 10% of all particles. This event is the origin of the common envelope surrounding both the Clouds, and of the turbulent gaseous filament connecting the main bodies of the Clouds, named the Magellanic Bridge (Brüns et al. 2005). Substantial fraction of the particles contributed to the Magellanic Stream as well.

The results summarized in the preceding paragraphs and depicted in Figure 16 have a remarkable consequence regarding the formation history of the Magellanic Stream. Over the last $\approx 3\,\mathrm{Gyr}$ it was supported at an almost constant rate by the gas tidally stripped from the Clouds. However, this rate was increased by a factor ≈ 20 due to a recent encounter between the Clouds at $t = -0.15\,\mathrm{Gyr}$. We would like to mention that on the qualitative level these results are an appropriate description of all the high–fitness models found in the parameter space for the LMC–SMC–Milky Way interaction.

We have found that the high–fitness simulations prefer the oblate ($q < 1$) shape of the logarithmic halo of the Galaxy over the prolate configuration (see Figure 5), but several reasonable models of q as high as 1.10 exist. As long as good models of the interacting system exist for the prolate halo, this shape of the Galactic gravitational potential cannot be ruled out. However, we have shown that such a possibility is substantially less likely than the case of $q < 1$. Moreover, only two acceptable models with significantly prolate ($q \gtrsim 1.10$) DM haloes of the Milky Way have been identified for a reasonable total mass of the halo, i.e. below the limit of $\approx 3 \cdot 12\,\mathrm{M}_\odot$ (see Section 3.1).

The impact of the flattening parameter on the phase–space positioning of the LMC/SMC orbits has been addressed in Section 6.4 of this paper. The shape of the Galactic halo also influences the redistribution of the matter associated with the Magellanic Clouds due to the resulting tidal field of the Milky Way. This effect is the key to the preference for the oblate configuration of the DM halo of our Galaxy. We have calculated the tidal force exerted by the Milky Way on two points separated by $\Delta r = 10\,\mathrm{kpc}$ and moving around the Galactic Center on circular polar orbits of the radii 50 kpc, 100 kpc and 150 kpc. Figure 17 shows the result. In general, the oblate configuration offers the most efficient tidal stripping, improving the probability that a sufficient redistribution of the LMC/SMC particles occurs within the available time–scale of several Gyr.

7. Summary and Conclusions

We have performed a detailed exploration of the parameter space for the interaction involv-

ing the Magellanic Clouds and the Milky Way. The method applied was similar to the approach by Růžička et al. (2009), but the results were quite different as a new free parameter was involved.

The recent work by Shattow & Loeb (2009) lead to the conclusion that the modified values of the LSR circular velocity and of the LSR angular rotation rate (Reid & Brunthaler 2004) introduce a significant change to the orbital history of the Magellanic Clouds. We have followed their study in order to show whether the large–scale distribution of H I in the Magellanic system can be simulated successfully even for the increased values of the LMC/SMC proper motions measured recently by Kallivayalil et al. (2006b,a) and by Piatek et al. (2008) if the revisited view of the galactic rotation (Reid & Brunthaler 2004) is adopted.

The study by Růžička et al. (2009) ruled out the tidal models of the LMC–SMC–Galaxy interaction because they were unable to reproduce the basic kinematic and morphological features of the most prominent structures originating in the Magellanic Clouds, i.e. of the Magellanic Stream and the Leading Arm (Brüns et al. 2005). Their automated analysis of the parameter space for the interaction has shown clearly that the recent proper motion measurements imply the past LMC/SMC orbits that allow for efficient tidal stripping of gas from the Clouds.

Unlike Růžička et al. (2009), we have taken into account the observational data by Reid & Brunthaler (2004) and treated the LSR circular velocity as a free parameter varied within the range $\Theta_0 = \langle 210, 260 \rangle \,\mathrm{km\,s^{-1}}$. Following Reid & Brunthaler (2004), a modified value of the LSR angular rotation rate Ω_0 of $29.45\,\mathrm{km\,s^{-1}\,kpc^{-1}}$ was adopted as well, yielding the studied range of the Solar galactocentric distance R_0 of $\langle 7.13, 8.83 \rangle\,\mathrm{kpc}$. As shown in Section 5 of this paper, the new values of Θ_0 and Ω_0 affect the galactocentric positions and velocities of the Magellanic Clouds, as well as the mass of the Galaxy.

The exploration of the modified parameter space for the interaction has revealed a remarkable qualitative change regarding the features of the resulting candidates for acceptable tidal models. The expectations of Shattow & Loeb (2009) have been confirmed because satisfactory reproduction of the large–scale Magellanic structures was possible for the LMC/SMC proper motion data by the HST. Moreover, such quality models have been localized for a large number of the proper motion combinations (Figure 4). This is due to the fact that the proper motions no longer play the exclusive role in establishing the actual 3 D galactocentric motion of the Clouds.

The LMC/SMC velocity (and position) vectors are determined not only by their proper motions but also by the LSR circular velocity and the LSR angular rotation rate. The current phase space coordinates of the Clouds are linked with the mass distribution of the Galaxy due to Θ_0 and Ω_0. As a consequence, a great variability and freedom have been introduced in the parameter space concerning the options to choose the orbits of the Magellanic Clouds allowing for the efficient tidal redistribution of mass resulting in the formation of the Magellanic Stream.

All the high–fitness models of the interaction localized in the studied parameter space involved two close LMC–SMC encounters within the last 4 Gyr. The first one occurred at the time $t < -2.5\,\mathrm{Gyr}$ and triggered the evolution of the Magellanic Stream. This encounter caused the tidal heating of the outer regions of the original LMC/SMC particle discs. Subsequently, the disturbed particles were spread along the orbital paths of the Clouds due to the tidal stripping by the gravitational field of the Galaxy.

The latter encounter was placed only as recently as $-150\,\mathrm{Myr}$ ($-250\,\mathrm{Myr} \lesssim t \lesssim -80\,\mathrm{Myr}$), but its impact on the LMC/SMC particles was at least by a factor of 10 stronger compared to the first encounter (for more rigorous discussion see Section 6.9). This event was also the beginning of the formation of the filament connecting the Clouds, composed of turbulent gas and young stars, called the Magellanic Bridge (Brüns et al. 2005). It is a notable fact that the recent encounter between the Clouds is a rather general feature of the interaction. Figure 12 demonstrates that it is likely an intrinsic property of the recent proper motion data. The studies by Kallivayalil et al. (2006b,a) and by Piatek et al. (2008) seem to introduce a LMC–SMC approach to the distance of $\approx 10\,\mathrm{kpc}$ at the time of $\approx -150\,\mathrm{Myr}$.

8. Discussion

Although it is usually assumed that a long–term gravitational binding between the Clouds has existed, we have confirmed the previous findings by Růžička et al. (2007, 2009) that such a condition is not necessary regarding the tidally induced redistribution of mass associated with the Clouds leading to the formation the Magellanic Stream. Figure 13 shows clearly that after the first encounter, the spatial separation of the Clouds usually exceeds 200 kpc.

The assumption of the Clouds being gravitationally bound is supported by several more observational indications. First of all, the Magellanic Clouds are surrounded by a low–density gaseous envelope which is a natural feature associated with two interacting bodies sharing a common history. However, we have found that the second of the mentioned LMC–SMC encounters is able to produce such a diffuse gaseous structure.

The gravitational binding of the Clouds is also often substantiated by their unique composition which is quite outstanding within the neighborhood of the Milky Way. Most of the satellites of the Galaxy are dwarf spheroidal while the LMC and the SMC are highly unevolved gas–rich irregular galaxies. The likelihood that such a couple was formed by chance in the Local Group of Galaxies is very small, obviously. These issues are serious, but they cannot be addressed within the framework of our parametric study.

It is one of the most surprising results of the genetic algorithm–based exploration of the parameter space that good models have been localized independently of the total mass of the Milky Way (see Figure 5). This behavior of the interacting system occurred due to the LSR circular velocity that links the present phase–space positions of the Clouds with the actual enclosed mass of the galactic DM halo. The consequence of such a complex nature of the system is nicely manifested by Figure 6.

However, even the remarkable reduction of the uncertainties of the LMC/SMC proper motions achieved by Kallivayalil et al. (2006b,a) and by Piatek et al. (2008) has left error boxes large enough to accommodate virtually every request for the proper motions to compensate the actual choice for the LMC circular velocity. Hence, the current phase–space positions of the Clouds can be selected in order to make the tidal model work over a wide range of the enclosed Galactic mass. Reasonable simulations of the Magellanic Stream have been made over the range of $0.6 \cdot 10^{12}\,\mathrm{M}_\odot$ to $3.0 \cdot 10^{12}\,\mathrm{M}_\odot$ for the total mass of the Milky Way enclosed within the radius of 250 kpc.

It cannot be omitted that as the Galactic mass decreases due to the decrease of the LSR circular velocity, the density profile of the DM halo steepens in the inner region of the Galaxy. This is caused by the rescaling of the rotation curve of the Milky Way yielded by the relation $\Omega_0 = \Theta_0/R_0 =$ const. Such behavior is helpful in respect to our goals, but it must be treated with care.

Besla et al. (2007) have pointed out that various observations have put constraints on the upper limit for the total mass enclosed within ≈ 50 kpc from the Galactic Center. However, taking such findings into account does not disprove our results. The limits on the total mass in the inner part of the Milky Way can be considered simply as additional constraints reducing the number of acceptable parameter combinations.

The redistribution of the matter associated with the Magellanic Clouds followed a scenario similar to that one by Gardiner et al. (1994). The formation of the Magellanic Stream (and of its natural counterpart – the Leading Arm) was triggered by a LMC–SMC encounter 2.5 Gyr ago. However, the Stream as old as ≈ 2 Gyr is at odds with the recent conclusions by Stanimirović et al. (2008) or by Bland-Hawthorn (2009). They argue that the interaction of the relatively cold H I of the Stream with the hot ambient halo of the Milky Way results in the thermal fragmentation (Stanimirović et al. 2008) and the ablation (Bland-Hawthorn 2009) of the H I clouds. Such a decay yields the maximum survival time of the H I clouds not exceeding ≈ 1 Gyr. However, our model introduces a continuous replenishment of the Stream gas, and a strong boost to this process due to the second LMC–SMC encounter at ≈ -0.15 Gyr.

We also have to point out the fundamental difference regarding the phase–space structure of the Magellanic Stream if the tidal and ram pressure models are compared. Mastropietro et al. (2005) have shown that the ram pressure–induced Stream possesses a rather compact phase–space structure. On the other hand, we have seen

that the tidal mechanism leads to the Magellanic Stream composed of several filaments of different ages. These filaments are the remnants of the past LMC/SMC orbital revolutions and might lie in significantly different distances even as large as 150 kpc (see Figures 15 and 16). Since the study by Stanimirović et al. (2008) assumed the Stream to lie not further than 50 kpc from the Galactic Center, their results cannot fully be applied to our models. The decay of the H I clouds due to the interaction with the hot gaseous halo of the Milky Way might be slower at larger radii as the density of the ambient Galactic medium falls with the galactocentric distance.

It is a challenging problem for the tidal models of the Magellanic System to explain the absence of stars in the Stream. Whilst evolutionary scenarios taking ram pressure stripping as the dominant process in the formation of the Magellanic Stream explain the problem naturally, tides affect both stars and gaseous clumps. Hence, the missing stars pose a serious issue regarding the tidal origin of the Stream.

The study by Bekki & Chiba (2009) has shown by the means of self–consistent numerical simulations that the key parameter determining the stellar content in a tidal model of the Magellanic Stream is the relative extent of gas and stars in the SMC. Assuming that the radii of the H I and stellar distributions in the SMC are of $2 \leq r_{\rm H\,I}/r_{\rm stars} \leq 4$, Bekki & Chiba (2009) have successfully reproduced the observed composition of the Magellanic Stream. The corresponding stellar distribution was disturbed by the recent ($t \approx -200$ Myr) LMC–SMC encounter and contributed to the extended SMC/LMC halos, but no stars appeared in the Magellanic Stream. The assumption on $r_{\rm H\,I}/r_{\rm stars}$ has a solid observational support, as the H I diameters of gas–rich galaxies are observed to be significantly larger than their optical disks (e.g. Broeils & van Woerden 1994).

Stars and gaseous clumps are treated identically as test particles in our model and they satisfy the same equations of motion. Whether a given particle represents a star or an H I cloud depends on its initial distance from the SMC (LMC) center and on the assumed radius of the stellar body. This quantity was estimated through the use of observational and theoretical constraints summarized in the previous paragraph and was set to $0.5 r_{\rm disk}$ (see Table 1).

The recent LMC–SMC encounter strongly affected the test particles within the radius of the stellar body, but similar to Bekki & Chiba (2009) most of the particles contributed to the common envelope of the Clouds. However, $< 5\,\%$ of such particles were moved to the Stream and may thus be considered its stellar contamination. Unfortunately, this is inevitable in a restricted N–body simulation. Our model overestimates the amount of matter stripped from the SMC center due to its over–simplified description, where self–gravity and dissipative gas dynamics will act against the tidal stripping as significant restoring forces (see Section 6.6).

9. Open questions

The values of the LSR circular velocity by Reid & Brunthaler (2004) certainly represent a progress towards the resolution of the difficulties arising from the recent HST proper motions of the Magellanic Clouds. However, we have not revealed a parameter set allowing for the correct modeling of the far tip of the Magellanic Stream. An offset of a model from the observations was present (Figure 15). This occurred because the LMC/SMC orbits have not crossed the corresponding region of the position–position–LSR radial velocity space. Nevertheless, we should keep in mind the simplicity of our model. Neither the dissipative hydrodynamical processes were included, nor did we account for the alternative scenarios such as the recent idea by Nidever et al. (2008).

They have analyzed the kinematics of the Magellanic Stream and the Leading Arm, with the focus on the transition regions between these structures and the main bodies of the Clouds. Their results suggest that both the Magellanic Stream and the structure LA I (Brüns et al. 2005) might be evolutionarily related to the region in the south–east of the LMC where a massive star formation takes place. It is possible that such a star forming activity has caused a strong blowout of gas which was later redistributed by the tidal or ram pressure stripping.

The scenario proposed by Nidever et al. (2008) might be the complementary process to the tidal stripping concerning the origin of the Leading Arm. While the tidal model succeeded reproduc-

ing the clumps LA II, LA III, the gas blow–out would transport gas to the position of the complex LA I. In general, such a process is able to eject gas with an arbitrary direction of its momentum with respect to the LMC motion. It might allow for filling the regions of the phase–space unreachable by the tidal/ram pressure models with gaseous matter.

We are grateful for the support by the FWF Austrian Science Fund (the grant P20593–N16), by the Academy of Sciences of the Czech Republic (the Junior research grant KJB300030801), and by the project MŠMT LC06014 Center for Theoretical Astrophysics. Our thanks go also to Christian Brüns who kindly provided excellent observational data, and to Matthew Wall for his advanced C++ library of genetic algorithms.

A. Fitness function

We have further improved the fitness function devised by Růžička et al. (2007) in order to handle the weaknesses of their scheme revealed later in the work by Růžička et al. (2009). The first component of our fitness function is still based on the approach by Theis & Kohle (2001) who proposed a generally applicable technique of comparing the relative intensities of the corresponding pixels in the modeled and observed data–cubes.

Both modeled and observed H I column density values are scaled relative to their maxima to introduce dimensionless quantities. Then, we get

$$f_1 = \frac{1}{N_v \cdot N_x \cdot N_y} \sum_{i=1}^{N_v} \sum_{j=1}^{N_y} \sum_{k=1}^{N_x} \frac{1}{1 + \left| \sigma_{ijk}^{\mathrm{obs}} - \sigma_{ijk}^{\mathrm{mod}} \right|}, \tag{A1}$$

where $\sigma_{ijk}^{\mathrm{obs}}$, $\sigma_{ijk}^{\mathrm{mod}}$ are normalized column densities measured at the position $[j, k]$ of the i–th velocity channel of the observed and modeled data, respectively. N_v is the number of separate LSR radial velocity channels in our data. $(N_x \cdot N_y)$ is the total number of positions on the plane of sky for which observed and modeled H I column density values are available.

The second component of the fitness function performs a search for structures in the position–position–velocity space of the data–cube. The modeled distribution of H I is compared to its observed counterpart regardless of the exact levels of the H I radio emission. It combines the enhancement of structures in the data by their Fourier filtering (see Růžička et al. 2007) with the subsequent check for empty/non–empty pixels in both data–cubes. The corresponding component of the fitness function is defined as follows:

$$f_2 = \frac{\sum_{i=1}^{N_v} \sum_{j=1}^{N_y} \sum_{k=1}^{N_x} \mathrm{pix}_{ijk}^{\mathrm{obs}} \cdot \mathrm{pix}_{ijk}^{\mathrm{mod}}}{\max\left(\sum_{i=1}^{N_v} \sum_{j=1}^{N_y} \sum_{k=1}^{N_x} \mathrm{pix}_{ijk}^{\mathrm{obs}}, \sum_{i=1}^{N_v} \sum_{j=1}^{N_y} \sum_{k=1}^{N_y} \mathrm{pix}_{ijk}^{\mathrm{mod}} \right)}, \tag{A2}$$

where $\mathrm{pix}_{ijk}^{\mathrm{obs}} \in \{0, 1\}$ and $\mathrm{pix}_{ijk}^{\mathrm{mod}} \in \{0, 1\}$ indicate whether there is matter detected at the position $[i, j, k]$ of the 3 D data–cube of the observed and modeled Magellanic System, respectively.

Růžička et al. (2007) showed that the search for structures significantly improves the performance of the genetic algorithm if the structures of interest occupy only a small fraction of the system's entire data–cube ($< 10\%$ in the case of the Magellanic Stream and the Leading Arm).

The fitness function f_2 is a measure for the agreement of the shape in the data. No attention is paid to the actual H I column density values. However, the efficiency of such a search for structures becomes lower with the increasing resolution of the compared data–cubes, as the relative number of non–empty pixels usually decreases in such a case, and the function f_2 returns very small values. To resolve the described difficulty, we have proposed a new component of the fitness function which is based on Equation (A2). In fact, we have introduced another simplification level for the view of the properties of the studied system. Similarly to Equation (A2) the number the overlapping non–empty pixels in the observed and modeled data–cubes is counted. This procedure is performed repeatedly for a series of N data–cubes of an increasing resolution. It is significantly easier to achieve a good match in case of low–resolution data, but the sensitivity to structures is rather poor, and only global positioning of the system as a whole is evaluated. High–resolution data provide more detailed information on the system, but the corresponding complexity prevents the comparison from driving the genetic algorithm efficiently. The newly designed component of the fitness function may be

described as

$$f_3 = \frac{\sum\limits_{m=0}^{N} 2^m \sum\limits_{i=1}^{N_\upsilon^m} \sum\limits_{j=1}^{N_y^m} \sum\limits_{k=1}^{N_x^m} \mathrm{pix}_{ijk}^{\mathrm{obs}} \cdot \mathrm{pix}_{ijk}^{\mathrm{mod}}}{\sum\limits_{m=0}^{N} 2^m \sum\limits_{i=1}^{N_\upsilon^m} \sum\limits_{j=1}^{N_y^m} \sum\limits_{k=1}^{N_x^m} \mathrm{pix}_{ijk}^{\mathrm{obs}}}, \tag{A3}$$

where N_x^m, N_y^m, and N_υ^m are the dimensions of the m–th data–cube and

$$N_x^m < N_x^{m+1} \wedge N_y^m < N_y^{m+1} \wedge N_\upsilon^m < N_\upsilon^{m+1}.$$

Obviously, we have introduced a weighting factor of 2^m in Equation (A3). It reflects the above discussion and strongly emphasizes the models that are able to satisfy the high–resolution observational data.

Růžička et al. (2007) also recommended and successfully applied a system–specific comparison. In the case of the Magellanic Clouds, the very typical linear radial velocity profile of the Stream including its high negative velocity tip was considered important. The slope of the LSR radial velocity function is a very specific feature, strongly dependent on the features of the orbital motion of the Clouds. We have slightly modified the original definition for the LSR radial velocity check by Růžička et al. (2007), and the fourth fitness function component is defined as

$$f_4 = \frac{1}{1 + \sum\limits_{i=\mathrm{x,y},\upsilon} \left| \frac{\mathrm{pix}_i^{\mathrm{obs}}(\upsilon_{\min}) - \mathrm{pix}_i^{\mathrm{mod}}(\upsilon_{\min})}{N_i} \right|}, \tag{A4}$$

where $\mathrm{pix}_i^{\mathrm{obs}}(\upsilon_{\min})$ and $\mathrm{pix}_i^{\mathrm{mod}}(\upsilon_{\min})$ are the pixels with the minima of the observed LSR radial velocity profile of the Magellanic Stream and its model, respectively. The resulting fitness function f combines the above defined components in the following way:

$$f = \frac{1}{4} \sum_{i=1}^{4} f_i. \tag{A5}$$

Our definition of the fitness function is different from the approach by Růžička et al. (2009). Moreover, the additional fitness component f_3 has been introduced by Equation (A3). Therefore, the value of the fitness function returned for the given model needs further analysis to clarify whether the identified local peaks of the fitness function correspond to satisfactory models. This means that every system has its own threshold value of the fitness function which needs to be defined.

REFERENCES

Bekki, K., & Chiba, M. 2005, MNRAS, 356, 680

Bekki, K., & Chiba, M. 2009, PASA, 26, 48

Besla, G., Kallivayalil, N., Hernquist, L., Robertson, B., Cox, T. J., van der Marel, R. P., & Alcock, C. 2007, ApJ, 668, 949

Binney, J. 1977, MNRAS, 181, 735

Binney, J., & Tremaine, S. 1987, Galactic dynamics, ed. Binney, J. & Tremaine, S.

Bland-Hawthorn, J. 2009, in The Galaxy Disk in Cosmological Context, Vol. 254, IAU Symposium, ed. J. Andersen, J. Bland-Hawthorn, & B. Nordström, 241–254

Broeils, A. H., & van Woerden, H. 1994, A&AS, 107, 129

Brüns, C., et al. 2005, A&A, 432, 45

Choi, J., Weinberg, M. D., & Katz, N. 2007, MNRAS, 381, 987

Connors, T. W., Kawata, D., & Gibson, B. K. 2006, MNRAS, 371, 108

Dehnen, W., & Binney, J. J. 1998, MNRAS, 298, 387

Fellhauer, M., et al. 2006, ApJ, 651, 167

Fujimoto, M., & Sofue, Y. 1976, A&A, 47, 263

Gardiner, L. T., & Noguchi, M. 1996, MNRAS, 278, 191

Gardiner, L. T., Sawa, T., & Fujimoto, M. 1994, MNRAS, 266, 567

Harris, J., & Zaritsky, D. 2006, AJ, 131, 2514

Holland, J. H. 1975, Adaptation in natural and artificial systems. an introductory analysis with applications to biology, control and artificial intelligence

Kallivayalil, N., van der Marel, R. P., & Alcock, C. 2006a, ApJ, 652, 1213

Kallivayalil, N., van der Marel, R. P., Alcock, C., Axelrod, T., Cook, K. H., Drake, A. J., & Geha, M. 2006b, ApJ, 638, 772

Kroupa, P., & Bastian, U. 1997, New Astronomy, 2, 77

Li, Y., & White, S. D. M. 2008, MNRAS, 384, 1459

Lin, D. N. C., Jones, B. F., & Klemola, A. R. 1995, ApJ, 439, 652

Mastropietro, C. 2009, in Magellanic System: Stars, Gas, and Galaxies, Vol. 256, IAU Symposium, ed. J. T. van Loon & J. M. Oliveira

Mastropietro, C., Moore, B., Mayer, L., Wadsley, J., & Stadel, J. 2005, MNRAS, 363, 509

Nidever, D. L., Majewski, S. R., & Burton, W. B. 2008, ApJ, 679, 432

Pedreros, M. H., Anguita, C., & Maza, J. 2002, AJ, 123, 1971

Piatek, S., Pryor, C., & Olszewski, E. W. 2008, AJ, 135, 1024

Růžička, A., Palouš, J., & Theis, C. 2007, A&A, 461, 155

Růžička, A., Theis, C., & Palouš, J. 2009, ApJ, 691, 1807

Reid, M. J., & Brunthaler, A. 2004, ApJ, 616, 872

Shattow, G., & Loeb, A. 2009, MNRAS, 392, L21

Stanimirović, S., Hoffman, S., Heiles, C., Douglas, K. A., Putman, M., & Peek, J. E. G. 2008, ApJ, 680, 276

Stanimirović, S., Staveley-Smith, L., & Jones, P. A. 2004, ApJ, 604, 176

Theis, C. 1999, in Reviews in Modern Astronomy, Vol. 12, Reviews in Modern Astronomy, ed. R. E. Schielicke, 309

Theis, C., & Kohle, S. 2001, A&A, 370, 365

van den Bergh, S. 2000, The Galaxies of the Local Group, ed. van den Bergh, S. (Cambridge)

van der Marel, R. P., Alves, D. R., Hardy, E., & Suntzeff, N. B. 2002, AJ, 124, 2639

Wannier, P., & Wrixon, G. T. 1972, ApJ, 173, L119+

This 2-column preprint was prepared with the AAS LaTeX macros v5.2.

TABLE 1
FREE PARAMETERS OF THE LMC–SMC–MILKY WAY INTERACTION

Parameter	Value	Comment
$(\alpha_{\rm lmc}, \delta_{\rm lmc})$	$(81.90^\circ \pm 0.98^\circ, -69.87^\circ \pm 0.41^\circ)$	Equatorial coordinates
$(\alpha_{\rm smc}, \delta_{\rm smc})$	$(13.2^\circ \pm 0.3^\circ, -72.5^\circ \pm 0.3^\circ)$	
$(m-M)_{\rm lmc}$	18.5 ± 0.1	Distance moduli
$(m-M)_{\rm smc}$	18.85 ± 0.10	
$\mu_{\rm W}^{\rm lmc}[{\rm mas\,yr^{-1}}]$	$\langle -2.11, -1.92\rangle$	Proper motion components
$\mu_{\rm N}^{\rm lmc}[{\rm mas\,yr^{-1}}]$	$\langle +0.39, +0.49\rangle$	
$\mu_{\rm W}^{\rm smc}[{\rm mas\,yr^{-1}}]$	$\langle -1.34, -0.69\rangle$	
$\mu_{\rm N}^{\rm smc}[{\rm mas\,yr^{-1}}]$	$\langle -1.35, -0.99\rangle$	
$v_{\rm rad}^{\rm lmc}[{\rm km\,s^{-1}}]$	262.2 ± 3.4	Line–of–sight velocities
$v_{\rm rad}^{\rm smc}{\rm km\,s^{-1}}$	146.0 ± 0.60	
$r_{\rm disk}^{\rm lmc}[{\rm kpc}]$	$\langle 9.0, 12.0\rangle$	Initial radii of the particle disks
$r_{\rm disk}^{\rm smc}[{\rm kpc}]$	$\langle 5.0, 8.0\rangle$	
$(i_{\rm lmc}, p_{\rm lmc})$	$(34.7^\circ \pm 6.2^\circ, 129.9^\circ \pm 6.0^\circ)$	Inclination and position angles of the particle disks
$(i_{\rm smc}, p_{\rm smc})$	$(60^\circ \pm 20^\circ, p = 45^\circ \pm 20^\circ)$	
$\Theta_0[{\rm km\,s^{-1}}]$	$\langle 210, 260\rangle$	LSR circular velocity
q	$\langle 0.71, 1.30\rangle$	Flattening of the DM halo of the Milky Way

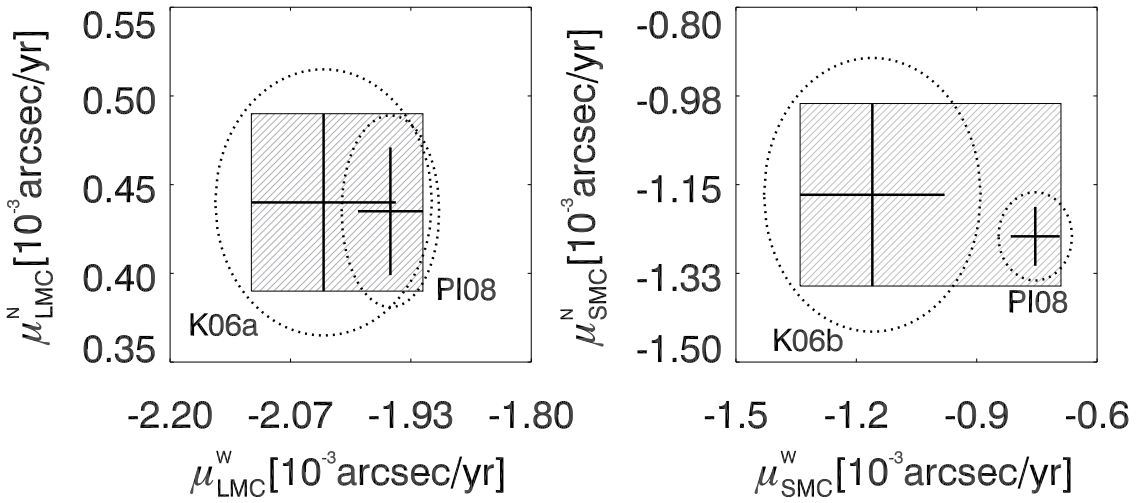

Fig. 1.— The 2 D projections of the Magellanic parameter space to the ($\mu^{\rm N}$, $\mu^{\rm W}$)–plane for both the LMC (left plot) and the SMC. The gray fillings mark the proper motion ranges explored by genetic algorithm. The labels indicate the proper motions as expected by the studies by Kallivayalil et al. (2006b)(K06a), Kallivayalil et al. (2006a)(K06b), and Piatek et al. (2008)(PI08). The ellipses show the 68.3 % confidence regions.

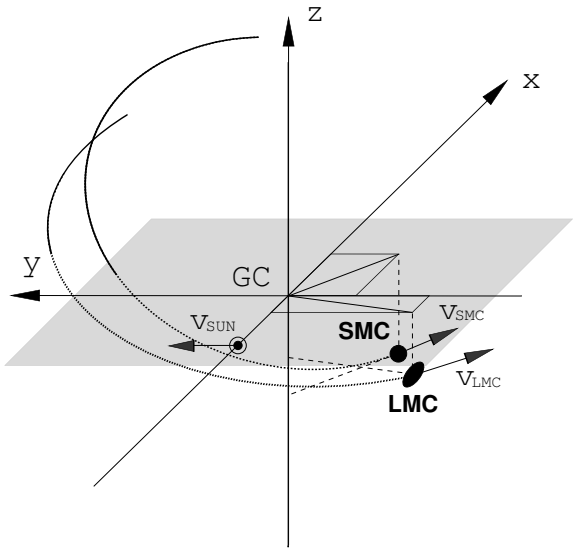

Fig. 2.— View of the Magellanic System. The positions of the Sun and of the Magellanic Clouds are shown in a galactocentric Cartesian frame. The frame was selected so that its z–axis coincides with the axis of the Milky Way disk and points towards the Northern Galactic Pole. The current Solar position vector is $\mathbf{R}_\odot = (-\Theta_0/\Omega_0, 0, 0)\,\mathrm{kpc}$, and the Sun is moving in the direction of the y–axis, i.e. $\boldsymbol{v}_\odot = (0, \Theta_0, 0)\,\mathrm{km\,s^{-1}}$. The Magellanic Clouds are $\approx$20 kpc far from each other, and their present day velocity vectors are almost parallel.

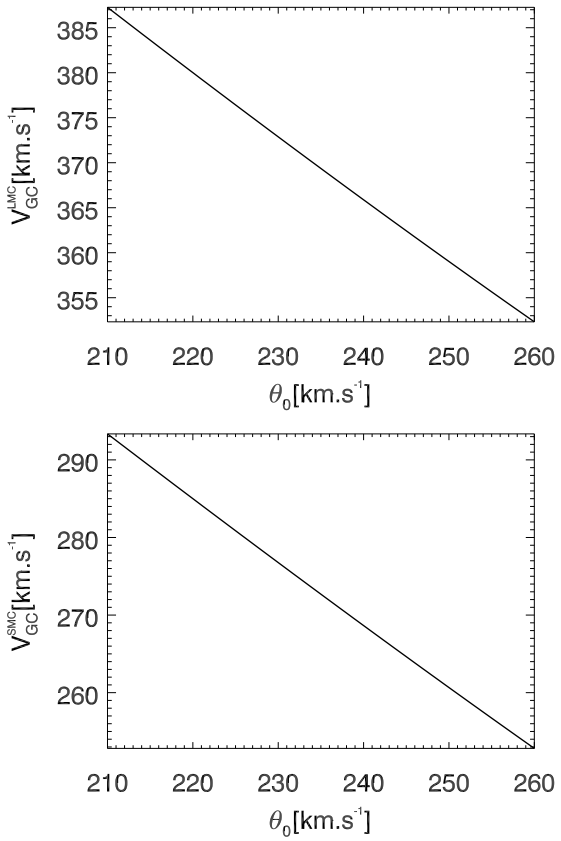

Fig. 3.— Galactocentric velocities of the Magellanic Clouds. The magnitude of the velocity vector of the LMC as a function of the LSR circular velocity is displayed in the upper plot. The lower plot shows the same relation for the SMC. Both plots assume the galactocentric coordinate frame depicted in Figure (2) and the LSR angular rotation rate $\Omega_0 = 29.45\,\mathrm{km\,s^{-1}\,kpc^{-1}}$ (Reid & Brunthaler 2004). Both Clouds slow down with respect to the Galactic Center if the LSR circular velocity is increased.

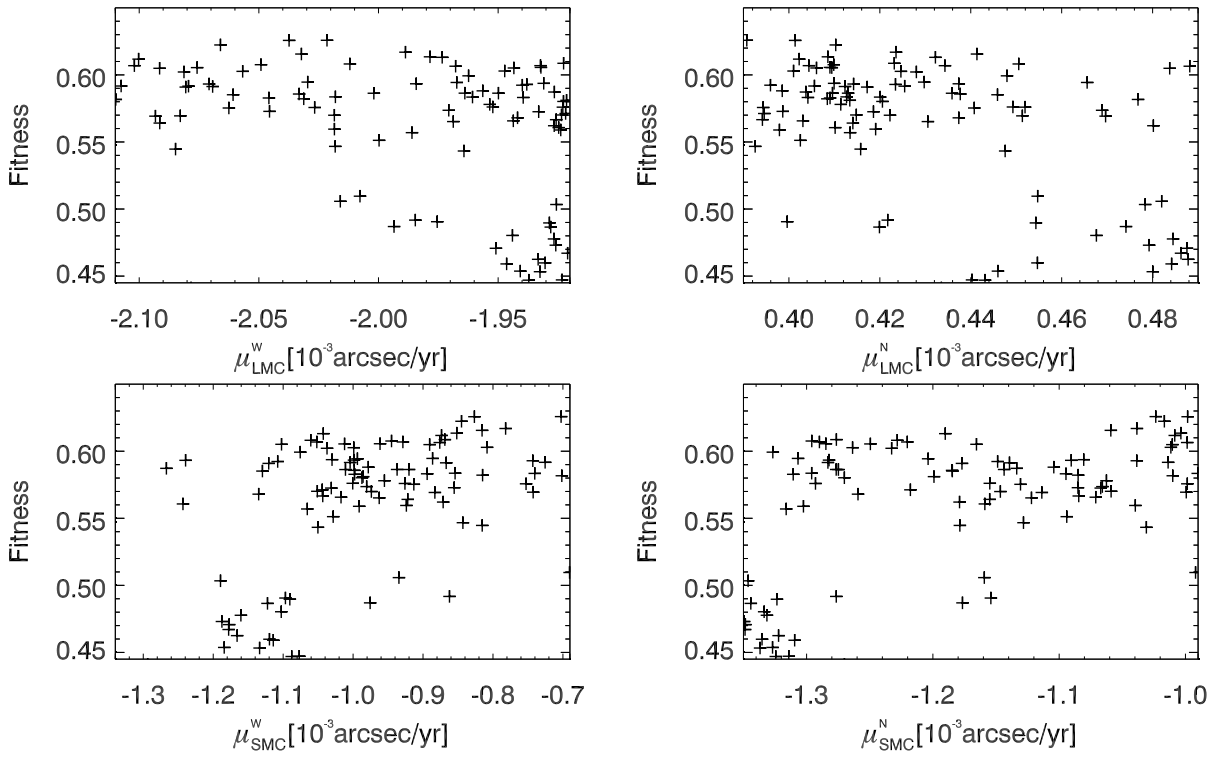

Fig. 4.— Distribution of all high–fitness models of the Magellanic System identified by the genetic algorithm. The upper row shows the fitness of the models as a function of the western (left plot) and of the northern LMC proper motion component, respectively. The lower row offers the same relations for the SMC.

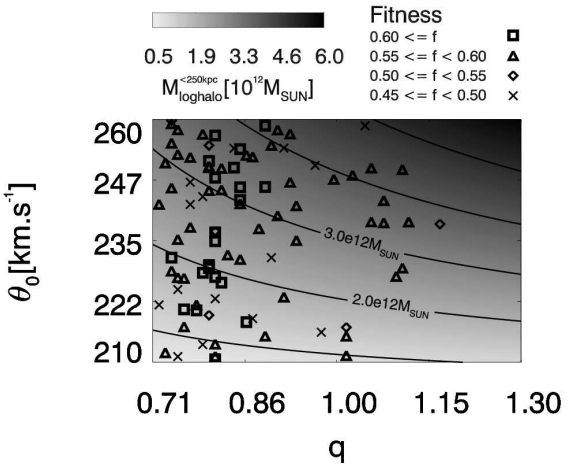

Fig. 5.— Total mass of the Milky Way enclosed within the radius of 250 kpc as a function of the LSR circular velocity Θ_0 and of the DM halo flattening q. All the high–fitness models identified by the genetic algorithm search are over–plotted according to their $[q, \Theta_0]$ positions. While no trend exists regarding the dependence on Θ_0, the models for oblate ($q < 1$) haloes are preferred.

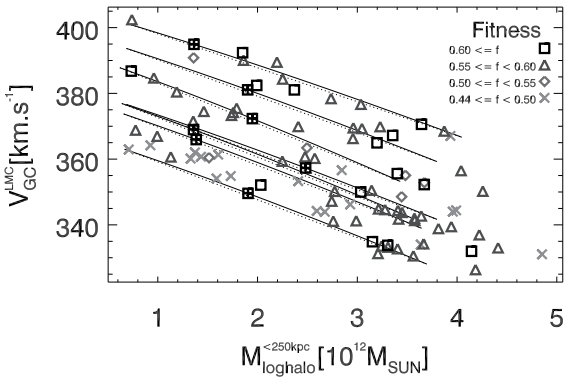

Fig. 6.— The galactocentric velocity of the LMC as a function of the total mass of the Milky Way. The models of the interaction between the Magellanic Clouds and the Galaxy which were identified by the genetic algorithm are divided into four groups regarding the value of their fitness. The curves (solid lines) corresponding to the parametric equations (18) and (19) are plotted for several randomly selected models of the fitness $f > 0.60$ (squares with crosses inside), i.e. for different combinations of the parameters q, $(\alpha_{\rm lmc}, \delta_{\rm lmc})$, $(m-M)_{\rm lmc}$, $(\mu_{\rm W}^{\rm lmc}, \mu_{\rm N}^{\rm lmc})$, and $\upsilon_{\rm rad}^{\rm lmc}$. The dotted lines demonstrate the proximity of the parametric curves to a linear relation.

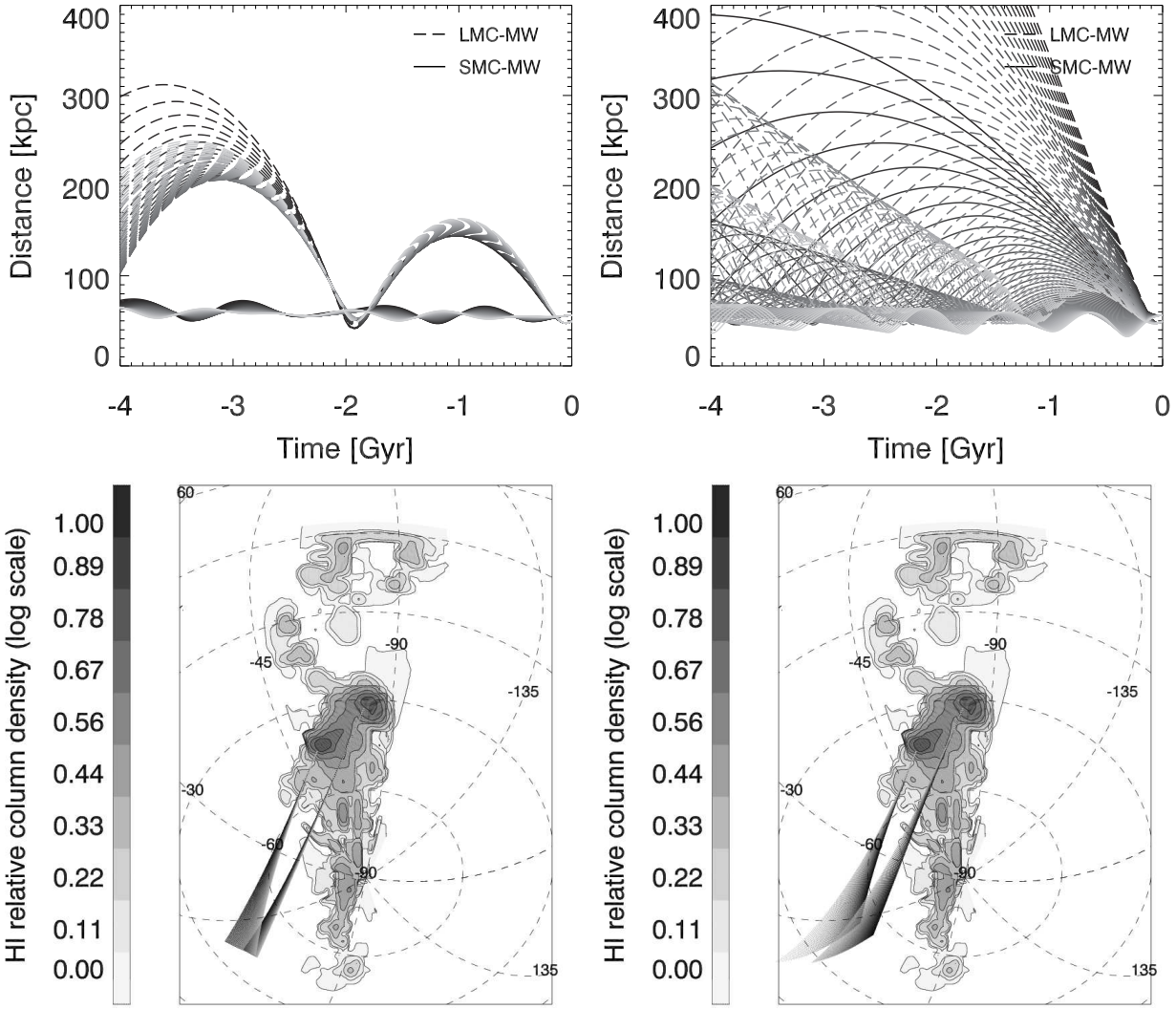

Fig. 7.— Orbits of the Magellanic Clouds as functions of the Milky Way halo flattening q (left column) and of the LSR circular velocity Θ_0, respectively. The parameter q was varied within the range of $\langle 0.71, 1.30 \rangle$ while Θ_0 was fixed to the value of $238\,\mathrm{km\,s^{-1}}$. When the LSR circular velocity was the variable ($\Theta_0 = \langle 210, 260 \rangle$), the flattening $q = 0.80$ was selected (right column). The upper row depicts the past time dependence of the LMC–Galaxy and the SMC–Galaxy distances. The plots in the lower row show the LMC (more to the right) and SMC orbits over the last 300 Myr projected to the plane of sky. Galactic coordinates are used. The color coding is such that the black to light gray transition corresponds to changing the actual variable from its minimum to its maximum. The contour maps shows the low resolution H I observations of the Magellanic Clouds and associated structures by Brüns et al. (2005).

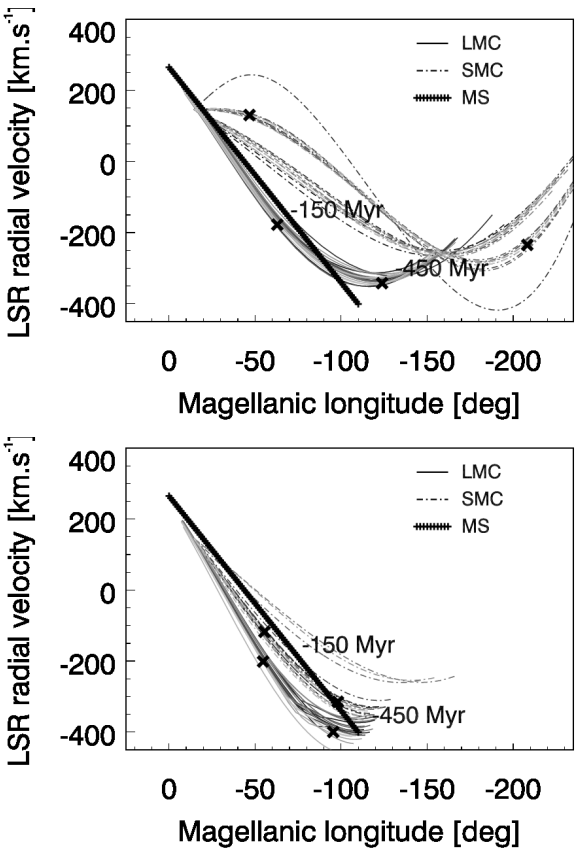

Fig. 8.— LSR radial velocity profiles along the orbital tracks of the Magellanic Clouds. The radial velocity is plotted as a function of the Magellanic longitude (see, e.g. Brüns et al. 2005) for the models identified by the genetic algorithm. The best models of $f > 0.60$ (upper plot) and the low–quality fits of $f < 0.50$ are shown, respectively. The past positions of the Magellanic Clouds are marked at the times of $-150\,\mathrm{Myr}$ and $-450\,\mathrm{Myr}$. The bold line stretched between the Magellanic longitudes of $0°$ and $-110°$ corresponds to the observed LSR radial velocity profile of the Magellanic Stream.

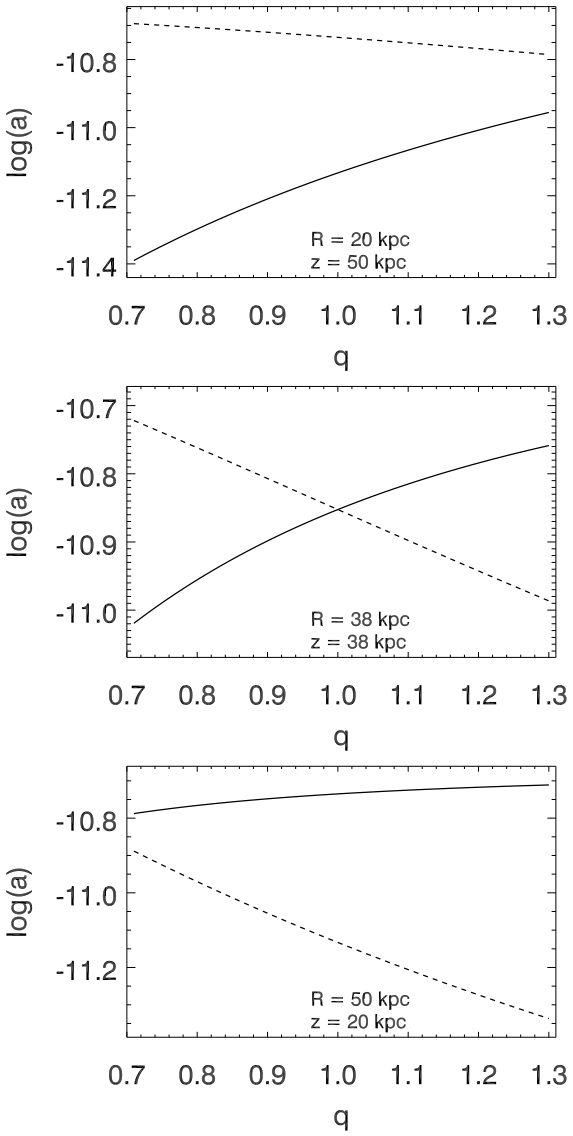

Fig. 9.— Intensity of the gravitational field of the logarithmic halo. The radial (solid line) and the z components of the gravitational acceleration due to the axially symmetric logarithmic halo of the Milky Way are plotted as functions of the halo flattening parameter q. The values and the ratio of the components of the gravitational acceleration depend on the position as well. The radial force increases if the halo flattening is increased while the axial component of the gravitational field decreases in such a case.

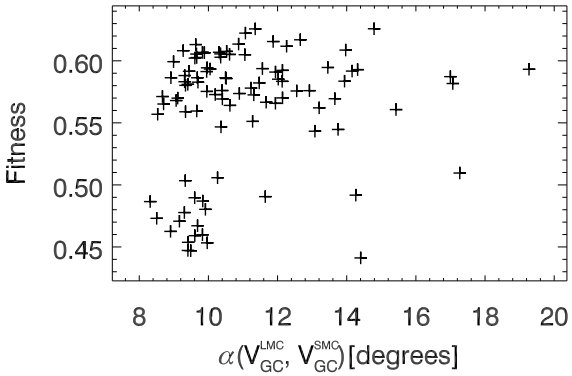

Fig. 10.— Fitness of the models identified by our evolutionary optimizer is plotted as a function of the scalar product of the current LMC and SMC velocity vectors. In most cases the deviation is smaller than 15°.

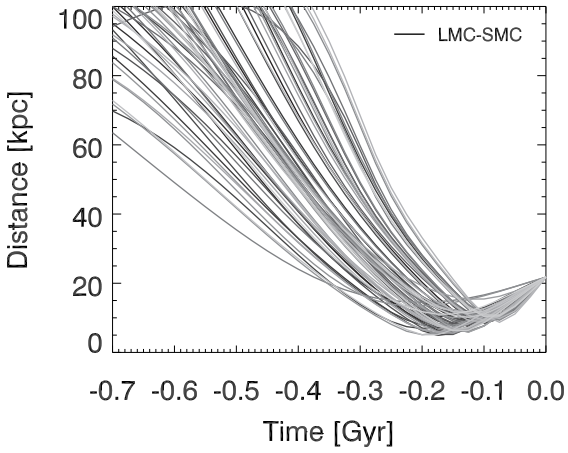

Fig. 11.— Time dependence of the distance between the centers of mass of the Magellanic Clouds. The function is plotted for the models of $f > 0.55$ back to the time of -0.7 Gyr. In all cases the LMC–SMC distance is increasing at present implying a minimum of the distance occurring in the past.

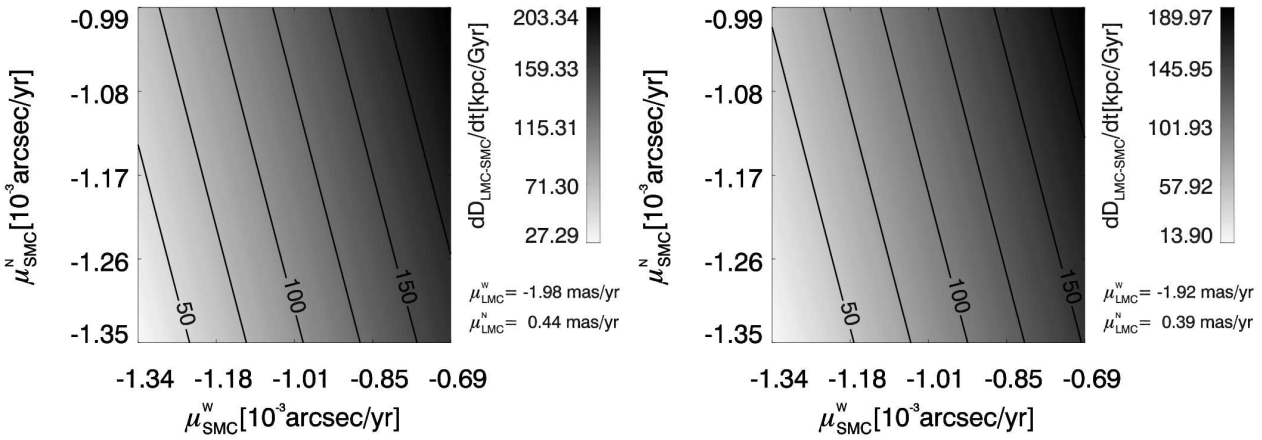

Fig. 12.— Current rate at which the distance between the Magellanic Clouds changes with time. The function $dD_{\rm l-s}/dt$ is plotted as a function of the SMC proper motion components $\mu_{\rm W}$ and $\mu_{\rm N}$. The proper motion components of the LMC correspond to those of a selected high–fidelity ($f > 0.60$) model (left plot), and to the limiting values of the ranges given by Equation (1), respectively. The minimum value for the western proper motion and the maximum of the northern LMC proper motion component were chosen to achieve the minimum spatial velocity. At present the rate $dD_{\rm l-s}/dt$ is positive. The distance between the Clouds is increasing.

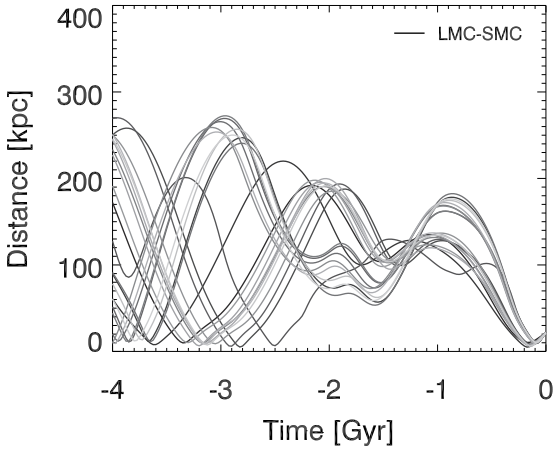

Fig. 13.— Time dependence of the distance between the centers of mass of the Magellanic Clouds. The function is plotted for the models of $f > 0.60$ back to the time of $-4.0\,\mathrm{Gyr}$. A close ($d \approx 15\,\mathrm{kpc}$) encounter between the LMC and the SMC occurred at $t < -2.5\,\mathrm{Gyr}$ in all cases despite the fact that the Clouds cannot be considered gravitationally bound to each other until the recent past.

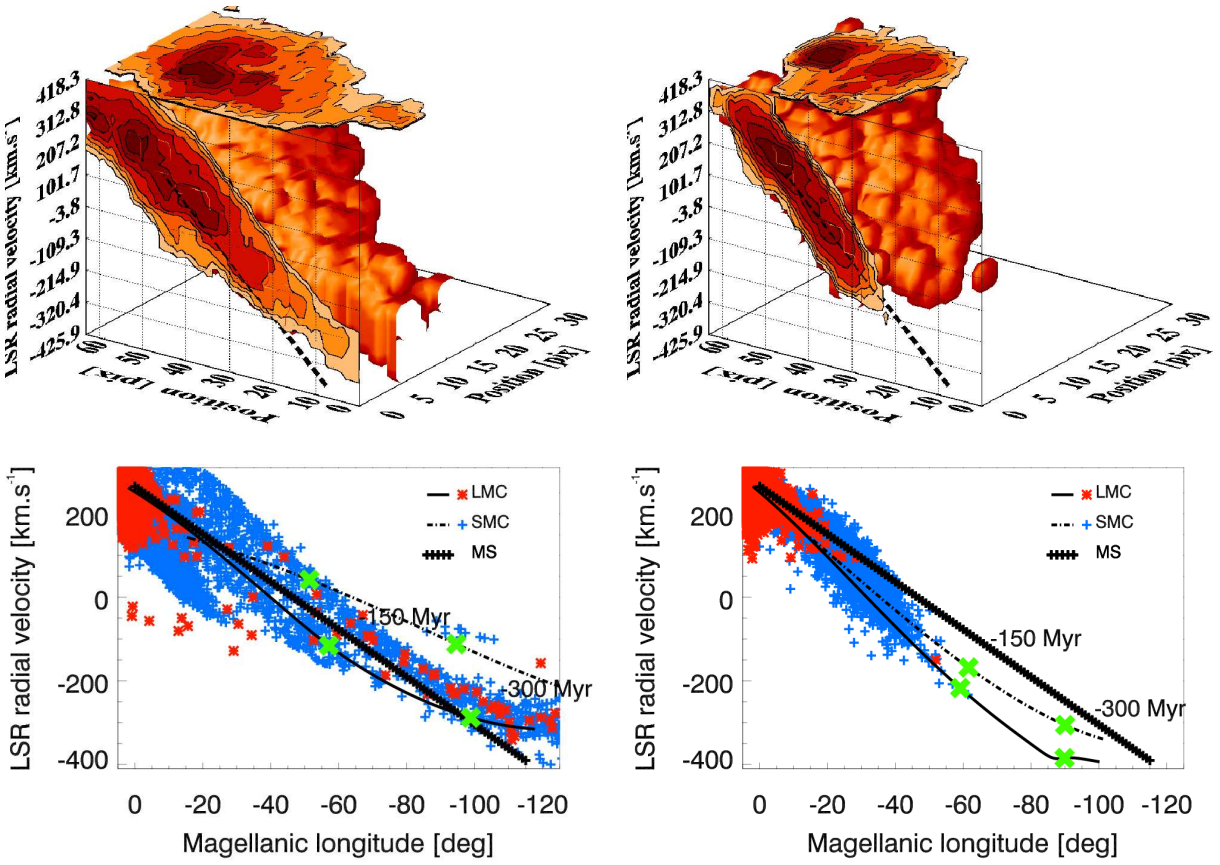

Fig. 14.— The threshold of the fitness function. The plots on the left hand side present an example of a satisfactory reproduction of the H I observations of the large–scale structures associated with the Magellanic Clouds (Brüns et al. 2005). The plots in the right hand column illustrate the typical output from a model for the LMC–SMC–Galaxy interaction that is not considered successful. The upper row of this figure offers the simulated low–resolution 3 D data–cube for both models. The column density isosurface of $\Sigma = 10^{-4}\Sigma_{\rm max}$ is depicted, together with the contour plots of the integrated relative column densities of H I projected to the position–position and position–LSR radial velocity spaces, respectively. The lower row provides a different view of the position versus LSR radial velocity dependence for the modeled Magellanic Stream. Positions of all individual LMC/SMC particles are plotted. Its LSR radial velocity profile is compared to the mean profile of the observed Stream (thick black line). For the definition of the Magellanic longitude, see Wannier & Wrixon (1972). Positions of the centers of mass of the Clouds are indicated at the time of −150 Myr and −300 Myr, respectively.

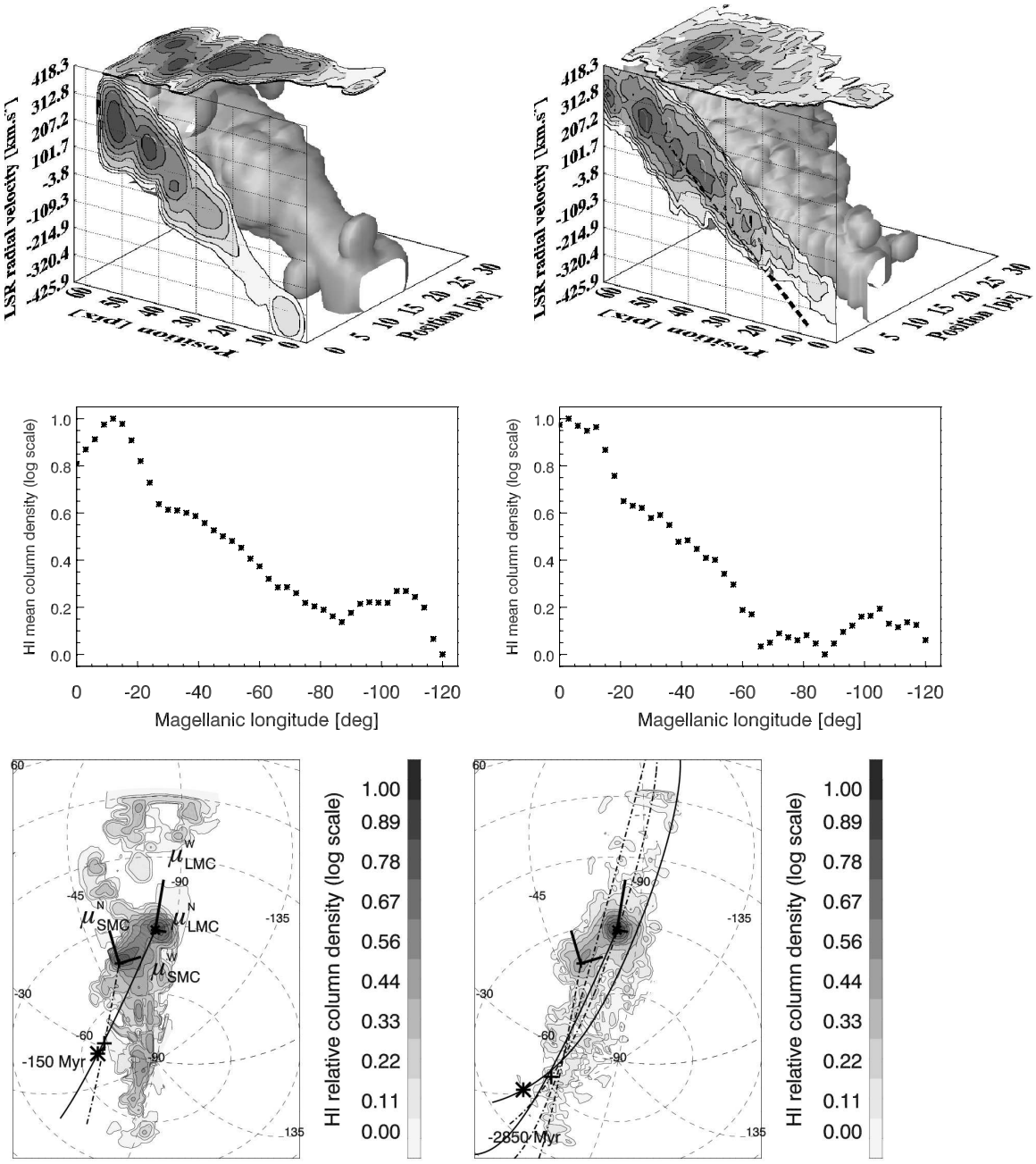

Fig. 15.— Large–scale distribution of H I associated with the Magellanic Clouds – observed versus simulated. The comparison of the observed (left column) low–resolution H I data–cube for the extended Magellanic structures (the Magellanic Stream, the Leading Arm) and of its modeled counterpart. The plots in the upper row depict the H I column density isosurfaces of $\Sigma = 10^{-4}\Sigma_{\rm max}$, and the contour plots of the integrated relative column densities of H I projected to the position–position and position–LSR radial velocity spaces, respectively. The middle row shows the mean column density of H I in the Stream as a function of the Magellanic longitude. The third row offers a detailed view of the integrated H I column densities projected to the plane of sky. The orbital tracks of the Clouds for the actual model are over–plotted over the last 300 Myr (lower left plot) and over the last 3 Gyr, respectively. The solid line corresponds to the past orbit of the LMC, while the dash–dotted line was used for the SMC. The present western and norther proper motions for both the Clouds are indicated.

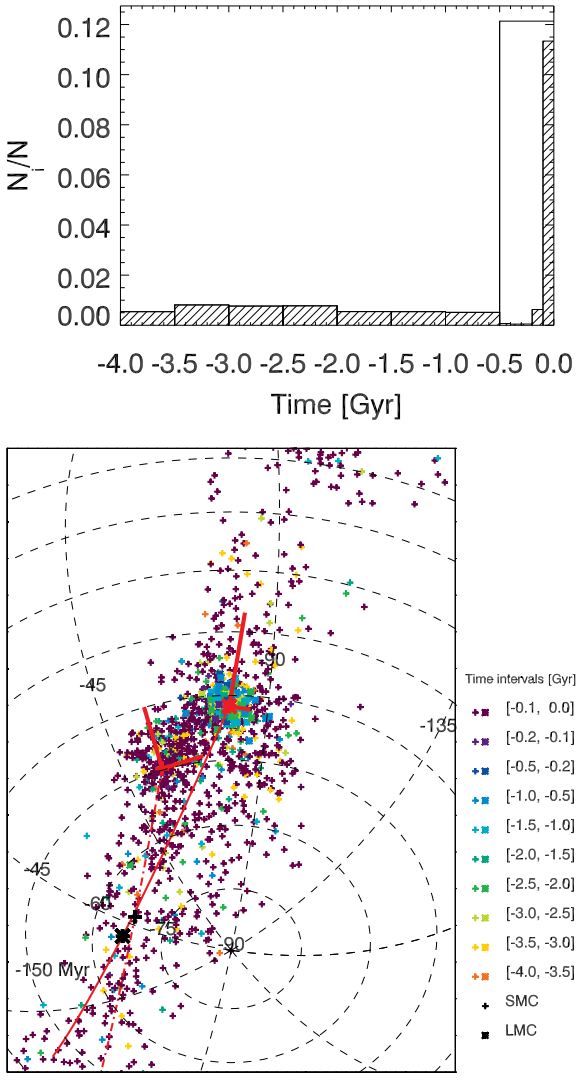

Fig. 16.— Relative number of the LMC/SMC particles strongly disturbed due to the encounter events in the LMC–SMC–Galaxy interaction for a high–fitness model of $f = 0.61$ (see also Figure 15). The upper plot shows the relative counts of the disturbed particles in eight bins of 500 Myr, starting at the time of -4 Gyr. The last bin is subdivided into five equal sections. The lower plot depicts the present distribution of the LMC/SMC particles. They are color–coded according to the epoch when they were stripped from the Clouds. The particles that remained bound to their galaxy of origin over the entire period of the simulation were not plotted. The Magellanic Stream is a composition of filaments of different ages spread along the past orbits of the Magellanic Clouds.

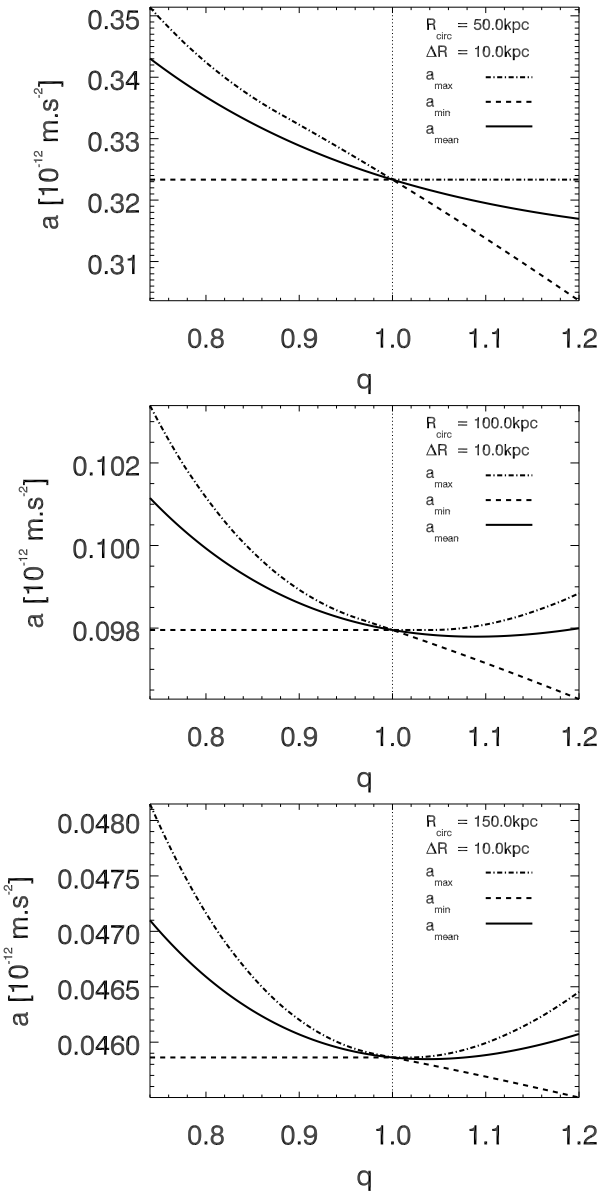

Fig. 17.— Tidal acceleration for an axially symmetric logarithmic potential as a function of its flattening parameter q. The values are calculated for two points on circular polar orbits of a constant radial distance $\Delta r = 10\,\mathrm{kpc}$. Three orbits of the radii of 50 kpc, 100 kpc and 150 kpc are shown, respectively. The plots show the mean value, the maximum and also the minimum of the acceleration on the given orbits.